Programa de doctorat en Física

Universitat de les Illes Balears

Growth laws and stable droplets close to the modulational instability of a domain wall

Damià Gomila Villalonga

Memòria d'investigació dirigida pel Dr. **Pere Colet Rafecas** *del Departament de Física Interdisciplinar del Institut Mediterrani d'Estudis Avançats.*

Desembre 2001.

Contents

Introduction

Spatially extended systems out of thermodynamic equilibrium typically undergo instabilities that lead to the formation of spatial inhomogeneities [1, 2]. In particular, we are interested here in the case in which the system may have several stable phases coexisting at the same time. The different regions occupied by the different phases are called domains, and they are delimited by fronts or interfaces (also called domain walls).

In systems momentarily driven out of equilibrium, spatial structures may appear as a transient until the system reaches thermodynamic equilibrium. In system permanently driven out of equilibrium spatial structures may appear as time-independent states or as dynamical states. Among the dynamical states, some of them are persistent (including those with spatio-temporal chaos), and others are transients towards a non-equilibrium stationary state. For systems approaching thermodynamic equilibrium or a non-equilibrium stationary state processes of domain growth and dynamical evolution of spatial structures can be studied. Systems for which growth processes have been studied include: simple and binary fluids, binary alloys, superfluids and superconductors, polymer blends, gels, lasers, optical cavities, geological systems (minerals), chemically reacting systems, metals, glasses and crystalline ceramics, order-disorder systems, magnetic systems, species segregation, and population growth in predator-prey systems. There are basically two types of growth in physical systems: interfacial or domain growth [3, 4] and growth by aggregation of similar particles [5]. In this work we will consider the former, that refers to the dynamical evolution of a system having various phases that coexist evolving towards a final state. The phase separation dynamics of a binary alloy following a quench below a critical temperature is a prototypical example of this situation. The dynamical evolution is governed by interface motion and the creation of topological defects. A relevant quantity in the domain growth process (called coarsening) is the average domain size, whose time-dependence gives a characteristic growth law.

Growth processes in the approximation to a final state of thermodynamic equilibrium are generally well-known [3]. Only recently, however, transient dynamics when the final state is not of thermodynamic equilibrium have been studied [6-14]. Two cases can be distinguished: systems for which a Lyapunov potential exist (potential systems) and systems for which do not (nonpotential systems). The definition of a Lyapunov potential is explained in detail in chapter 1.

In potential systems, the Lyapunov potential [15] plays the role of a free energy, so that the relative stability between asymptotic states can be measured. Thus, the general behaviour of a potential system, when the asymptotic states are homogeneous, is qualitatively identical to that of systems approaching thermodynamic equilibrium. However, in potential systems the asymptotic states are not necessarily homogeneous but they may contain spatial structures. In this case the dynamics of the interfaces is affected by the inhomogeneities of the asymptotic states.

In one dimension, the direction of motion of an isolated front is determined through the relative stability of the two asymptotic solutions. Specifically the front velocity is proportional to the Lyapunov potential difference and the detailed shape of the interface does not play an important role. Therefore, when the two asymptotic states are equivalent, and isolated wall between the two states do not move. If one or both phases are inhomogeneous, the movement of the front is affected by the modulation of the asymptotic states. As the front move, it feels a spatial dependent force generated by the inhomogeneities. Thus the velocity of the front becomes also modulated. If the asymptotic states have similar values of the potential, so that in principle a front should move slowly, the modulated force may lock the front at certain positions leading to a stationary front between the two slightly nonequivalent states. These structures are called Pomeau fronts [16]. In large systems with several walls between homogeneous asymptotic states, short-range interactions due to the tails of the fronts may come into play [17, 18]. In general, these interactions are negligible in the case of nonequivalent states as compared with the force associated to the Lyapunov potential difference, but they may manifest in the case of equivalent states or states with very similar values of the potential. When the profile of the front approaches monotonically the asymptotic states, the interaction between two walls is attractive and, for equivalent states, a domain delimited by two of these fronts tends to contract until the domain walls annihilate each other. When the front profiles show damped spatial oscillations, it is known that the interaction can involve both attractive and repulsive forces. Thus, oscillating domain walls may not annihilate each other, but they may locate at a certain distances where an equilibrium of forces occurs. This leads to a frozen steady state configurations due to the random pinning of interfaces [18].

In two dimensions the curvature of the wall of the domain plays an important role. In the case of equivalent homogeneous asymptotic states, the system tends to reduce the excess of energy located at the interfaces by decreasing their length. As shown in chapter 3, the normal front velocity v turns out to be proportional to the local curvature κ ($v = -\gamma\kappa$). As a consequence, if $\gamma > 0$, a circular domain of radius R ($v = dR/dt$ and $\kappa = 1/R$) tends to reduce its radius with the growth law $R(t) \sim \sqrt{R(t=0)^2 - \gamma t^{1/2}}$. Equivalently, arbitrarily shaped closed domains shrink and the system coarsens in a self-similar way (see Fig. (3.1)). This means that the domain structure is, in a statistical sense, independent of time up to a global scale factor: the system exhibits dynamical scaling. The characteristic domain size L evolve in time following the power law $L \sim t^{1/2}$ [14, 19, 20]. This simple description is modified when conservation laws restrict the dynamics leading to the $t^{1/3}$ power law [21]. In other cases the presence of walls may be energetically favored. In this case (negative surface tension) $\gamma < 0$ and the system prefers to have as long walls as possible. Thus, a flat wall becomes modulationally unstable and the system develops labyrinthine patterns [22, 23, 24]. When the asymptotic states are not homogeneous, the problem of domain growth in two dimensions is in much harder and only a few cases have been studied in the literature, either for potential or nonpotential systems [6, 25].

In the case of nonequivalent phases the main source of movement of the walls in two dimensions is the 1d mechanism explained previously. In diffusive systems, in general, the curvature acts to smooth out short-wavelength perturbations in the course of propagation [26]. In some cases, however, the shrinking effect of the curvature may counterbalance the expansion of a more stable phase into a less stable one. In this case an stationary radius for a circular domain exist. However, in the absence of any other mechanism, it is always unstable (nucleation theory) [3]. More complex mechanisms have been used to explain the existence of stable radius in a analogous situation in reaction-diffusion systems, as well as describe modulational instabilities of propagating fronts [22].

In two dimensions the short-range interactions due to the tails of the front are, in general, negligible as compared with the curvature driving force. However, when the interfaces are very close to each other and the system is in a parameter region where the curvature driving force is not so high, the oscillatory tails may cause the interfaces to be mutually repelling, thus stopping their movement due to the curvature. The repulsive forces induced by spatial oscillations may lead to the stabilization of a closed domain of a stable phase at a certain radius. The result is a localized structure (LS) [24]. The same explanation can been used to describe LS in nonpotential systems [10, 11, 27]. The oscillatory tails plays also an important role in the formation of labyrinthine patterns.

For systems without a Lyapunov potential the study of domain growth and domain wall motion is by far more complicate. The study of front propagation can no longer be done in terms of a free energy. It is known that a domain wall between two equivalent states may move in one dimension in either directions due to non-potential dynamics [28, 29]. In two dimensions more complicated effects may appear. Despite the fact that many physical systems of interest out of equilibrium are governed by nonpotential dynamics, there is no universal characterization of domain growth dynamics in two dimensions. There is presently only a partial understanding of a variety of possible situations [6, 14, 26]. In particular a number of results have been recently reported for domain growth and domain wall motion in the transverse plane of nonlinear optical systems [9-13]. Existence of dynamical scaling has been numerically shown only in [10, 11], where a $t^{1/2}$ power law has been found, but no derivation of such a law has been given for these systems.

The main objective of this work is to provide a universal description for the motion of domain walls in 2d nonpotential systems, at least for the simplest case of walls between asymptotic stable stationary homogeneous solutions that do not move in 1d. We establish rigorously the different growth laws for each different region of the parameter space and show in which regions there is dynamical scaling yielding to a power law and in which regions the growth does not follow a simple power law.

As a consequence we are able to characterize properly different phenomena related to interface dynamics such as the modulational instability of a flat domain wall and the transition from a coarsening regime to a labyrinthine pattern. Also we show the existence of a novel class of localized structures, the stable droplets, which have a very large radius and for which, at difference of typical localized structures, the tails of the front does not play any role in the stability of the droplet.

This report is organized as follows: In chapter 1 we define properly potential systems and we give a short classification of dissipative dynamical systems.

In chapter 2 we classify the different types of fronts between two homogeneous equivalent states.

In chapter 3 we give a brief summary of domain wall motion in potential systems in the case of fronts connecting two homogeneous equivalent states, which is the most interesting for comparison with the nonpotential case developed in detail in chapter 4.

Chapter 4 is devoted to the study of domain wall motion in nonpotential systems. We present a general description of domain wall motion for a very general class of systems. We develop a perturbation theory in order to obtain an equation for the velocity of the fronts (eikonal equation). We characterize then the transition from the regime characterized by a $t^{1/2}$ growth law to the one of labyrinthine pattern formation due to a modulational instability of a flat domain wall and derive an amplitude equation for the curvature by means of a multiple scale analysis. This analysis predict the existence of stable circular domain walls with large radius and regimes of domain wall motion with growth laws different from the $t^{1/2}$ power law. We illustrate our general results in a prototypical model: the parametrically driven complex Ginzburg-Landau equation.

Finally the main conclusions of the work and an outlook of future perspectives are presented in chapter 5.

Chapter 1

Potential and nonpotential systems

Potential systems are characterized by the existence of a potential functional or Lyapunov potential, whose minima characterize the asymptotic states of the system. The system evolves in time approaching the minima of the potential, and once it reaches one of such minima, it remains nearby as long as perturbations on the system are not too large. If $\mathcal{F}$ is a Lyapunov functional (in general, the Lyapunov potential will act on a space of dynamical functions $\vec{A}$), it must satisfy the relation [30]:

$$\frac{\mathrm{d}\mathcal{F}[\vec{A}]}{\mathrm{d}t} \leq 0, \tag{1.1}$$

and $\mathcal{F}$ bounded from below, which guarantees that the (nondegenerate) minima of $\mathcal{F}$ are stable fixed points of the dynamics. The absolute minimum of $\mathcal{F}$ is often called the stable state, while the other minima are referred as metastable states. It may occur that the dynamics is not purely relaxational and a residual dynamics comes into play once the relaxational part has taken the system to a minimum of $\mathcal{F}$.

In a quite general way, we can write the time evolution equation of dynamical variables describing a dynamical system as [31, 32]

$$\partial_t A_i(\vec{x}, t; \{\alpha\}) = -B_i^j \frac{\delta \mathcal{F}}{\delta A_j^*} + v_i[\vec{A}], \tag{1.2}$$

where $\vec{A}(\vec{x}, t; \{\alpha\})$ is the vector of dynamical variables (in general, functions or complex fields of the space coordinates, time and a set of parameters) defined in a Hilbert space $\mathcal{H}$, $\mathcal{F}$ is a real scalar functional $\mathcal{F} : D \subseteq \mathcal{H} \longrightarrow \mathbb{R}$, and $B\left(\vec{A}(\vec{x}, t; \{\alpha\})\right)$ is a positive operator [1].

On the basis of the decomposition (1.2) we can make a classification of potential systems as follows [14, 31]:

[1] An operator $\mathcal{L}$ defined in a Hilbert space $\mathcal{H}$ (on $\mathbb{C}$) is said to be positive when $\langle v, \mathcal{L}v\rangle \geq 0$, $\forall v \in \mathcal{H}$, being $\langle \cdot, \cdot \rangle$ the scalar product in $\mathcal{H}$. Moreover, this definition tacitly demands the hermiticity of $\mathcal{L}$.

- When $\vec{v} = 0$, the dynamics is purely relaxational and $\mathcal{F}$ is a Lyapunov functional. The way the system relaxes towards the minima of $\mathcal{F}$ depends on the peculiarities of the self-adjoint operator B. We can distinguish two cases:

  – **Relaxational gradient potential flow**. The operator B is a multiple of the identity. The system evolves following the lines of maximum slope (steepest descent) of $\mathcal{F}$, which plays the role of a free energy. A well-known example is the Ginzburg-Landau equation (GL) for a real field $\psi(\vec{x}, t)$ or model A dynamics (without noise):

$$\partial_t \psi = \nabla^2 \psi - V'(\psi), \tag{1.3}$$

where $V(\psi) = (1 - \psi^2)^2$ has a double well structure. This equation gives the dynamical evolution of a system described by a nonconserved scalar order parameter. It provides a suitable coarse-grained description of the Ising model (continuous version), as well as of binary alloys that undergo an order-disorder transition on cooling through a critical temperature. It is straightforward to see that eq. (1.3) can be rewritten in the form:

$$\partial_t \psi = -\frac{\delta \mathcal{F}_{\mathrm{GL}}}{\delta \psi}, \tag{1.4}$$

$$\mathcal{F}_{\mathrm{GL}}[\psi] = \int \mathrm{d}\vec{x} \left[\frac{1}{2} (\nabla \psi)^2 + V(\psi) \right]. \tag{1.5}$$

Another example of relaxational gradient potential flow is the real Swift-Hohenberg equation (SHE),

$$\partial_t \psi = \psi - (\nabla^2 + k_0^2)^2 \psi - \psi^3, \tag{1.6}$$

where k_0 is a system parameter. This is the simplest model equation describing a Turing instability [33] in systems with a real order parameter $\psi(\vec{x}, t)$. First derived as an order parameter equation for Rayleigh-Benard convection [34], it finds also application for the description of various pattern forming systems including nonlinear optical systems such as the nascent bistability [35], or degenerate optical parametric oscillators and degenerate four wave mixing [36]. Equation (1.6) has the gradient form

$$\partial_t \psi = -\frac{\delta \mathcal{F}_{\mathrm{SH}}}{\delta \psi}, \tag{1.7}$$

$$\mathcal{F}_{\mathrm{SH}}[\psi] = \int \mathrm{d}\vec{x} \left[\frac{1}{2} [(\nabla^2 + k_0^2)\psi]^2 - \frac{\epsilon \psi^2}{2} + \frac{\psi^4}{4} \right]. \tag{1.8}$$

The SHE has a fourth order spatial derivative, which may change qualitatively the dynamics of the domain walls with respect to the diffusive case (1.3). These differences will be discussed in chapter 3.

– **Relaxational nongradient potential flow**. In this case the operator B is not multiple of the identity and the dynamics does not follow the lines of maximum slope of $\mathcal{F}$. The Cahn-Hilliard equation or model B dynamics (without noise) constitutes a well-known example:

$$\partial_t\psi = -\nabla^2\left[\nabla^2\psi - V'(\psi)\right] = -\nabla^2\left(-\frac{\delta\mathcal{F}_{\mathrm{GL}}}{\delta\psi}\right). \tag{1.9}$$

This system corresponds to a conserved scalar order parameter and it models, for instance, phase separation in a binary alloy.

- **Nonrelaxational potential flow**. Now $\vec{v} \neq 0$ but $\mathcal{F}$ is still a Lyapunov potential. The first term on the rhs of (1.2) represents the relaxational part of the dynamics and the functional $\vec{v}[\vec{A}]$ corresponds to the residual dynamics. Most of the models used in equilibrium critical dynamics are of this type. In order to be $\mathcal{F}$ a Lyapunov potential the relation (1.1) must be satisfied

$$\begin{aligned}\frac{\mathrm{d}\mathcal{F}}{\mathrm{d}t} &= \int \mathrm{d}\vec{x}\,\frac{\delta\mathcal{F}}{\delta\vec{A}^*}\cdot\partial_t\vec{A}^* + \mathrm{c.c.}\\ &= -\int \mathrm{d}\vec{x}\,\left(\frac{\delta\mathcal{F}}{\delta\vec{A}}\right)^*\cdot B\left(\frac{\delta\mathcal{F}}{\delta\vec{A}}\right) + \int \mathrm{d}\vec{x}\,\left(\frac{\delta\mathcal{F}}{\delta\vec{A}}\right)^*\cdot\vec{v}[\vec{A}]^* + \mathrm{c.c.}\\ &= -2\left\langle\delta_{\vec{A}}\mathcal{F},\ B\,\delta_{\vec{A}}\mathcal{F}\right\rangle + 2\,\mathrm{Re}\Big(\left\langle\vec{v}[\vec{A}]^*,\ \delta_{\vec{A}}\mathcal{F}\right\rangle\Big) \le 0,\end{aligned} \tag{1.10}$$

being $\langle\cdot,\cdot\rangle$ a scalar product defined in $\mathcal{H}$ as $\langle\vec{f},\vec{g}\rangle = \int \mathrm{d}\vec{x}\,\vec{f}^*\cdot\vec{g}$, $(\delta\mathcal{F}/\delta\vec{A})_i \equiv \delta\mathcal{F}/\delta A_i$ and $\delta_{\vec{A}}\mathcal{F} \equiv \delta\mathcal{F}/\delta\vec{A}$; "c.c." stands for the complex conjugate. Since B is positive self-adjoint, the first term of the last part of (1.10) is less or equal than zero. Hence, a *sufficient* condition for $\mathcal{F}$ to be a Lyapunov functional is

$$\begin{aligned}\mathrm{Re}\Big(\left\langle\vec{v}[\vec{A}]^*,\ \delta_{\vec{A}}\mathcal{F}\right\rangle\Big) &= \int \mathrm{d}\vec{x}\,\frac{\delta\mathcal{F}}{\delta\vec{A}^*}\cdot\vec{v}[\vec{A}]^* + \mathrm{c.c.}\\ &= \int \mathrm{d}\vec{x}\,\frac{\delta\mathcal{F}}{\delta\vec{A}^*}\cdot\left[\partial_t\vec{A}^* + B\,\frac{\delta\mathcal{F}}{\delta\vec{A}}\right] + \mathrm{c.c.} = 0.\end{aligned} \tag{1.11}$$

An example for a complex field ψ is:

$$\partial_t\psi = -(1+i)\,\frac{\delta\mathcal{F}_{\mathrm{GL}}}{\delta\psi^*}. \tag{1.12}$$

It is easy to check that $\mathcal{F}_{\mathrm{GL}}$ is a Lyapunov functional:

$$\begin{aligned}\frac{\mathrm{d}\mathcal{F}_{\mathrm{GL}}}{\mathrm{d}t} &= \int \mathrm{d}\vec{x}\,\frac{\delta\mathcal{F}_{\mathrm{GL}}}{\delta\psi^*}\,\partial_t\psi^* + \mathrm{c.c.} = -(1-i)\int \mathrm{d}\vec{x}\,\frac{\delta\mathcal{F}_{\mathrm{GL}}}{\delta\psi^*}\,\frac{\delta\mathcal{F}_{\mathrm{GL}}}{\delta\psi} + \mathrm{c.c.}\\ &= -2\int \mathrm{d}\vec{x}\,\left|\frac{\delta\mathcal{F}_{\mathrm{GL}}}{\delta\psi}\right|^2 \leqslant 0.\end{aligned} \tag{1.13}$$

This case corresponds to $B = 1$, $\vec{v} = -i(\delta\mathcal{F}_{\mathrm{GL}}/\delta\psi^*)$; the dynamics can be decomposed into a relaxational gradient flow plus a term corresponding to a conservative Hamiltonian dynamics.

The *orthogonality condition* (1.11) can be proved to be equivalent to a Hamilton-Jacobi equation [37]. Its solution is in general cumbersome, although it can be obtained in some cases [38, 39, 40]. If nontrivial solutions for $\mathcal{F}$ of (1.11) are found, we can say that the system is potential. Otherwise, nothing can be guaranteed. In practice, we will say that a system is **nonpotential** when a decomposition of the dynamics in the form (1.2) cannot be found with a nontrivial $\mathcal{F}$ (that is, nonconstant) that decreases in time, although we do not proof that a Lyapunov potential does not exist. An illustrative example is the complex Ginzburg-Landau equation (CGLE)

$$\partial_t A = (1+i\alpha)\nabla^2 A + (\mu + i\nu)A - (1+i\beta)|A|^2 A, \tag{1.14}$$

whose dynamics was classified as nonpotential for a long time (except for limiting cases) until Graham and coworkers, at least in a range of parameters, were able to find an approximate nontrivial solution for (1.11), hence showing that in this regime the system dynamics may be characterized in terms of a Lyapunov potential [41, 42]. In reference [31] a detailed discussion about the numerical validity of such approximation can be found.

A lot of examples of nonpotential systems appear in the field of nonlinear optics. In particular, many models for nonlinear optical cavities are, in general, nonpotential. In these systems, the light in the transverse plane to the propagation is described by two dimensional partial differential equations of complex fields similar to the CGLE. Note, however, that the spatial coupling in optics comes through diffraction, which in the paraxial approximation is described by a Laplacian with a purely imaginary coefficient, so that diffusion is not present. As we will show in chapter 4, this will have important consequences for the dynamics of domain walls.

In potential systems, the Lyapunov functional gives information about global stability. If two fixed points $\vec{A}_i(\vec{x};\{\alpha\})$, $\vec{A}_j(\vec{x};\{\alpha\})$ are such that $\mathcal{F}[\vec{A}_i] \leqslant \mathcal{F}[\vec{A}_j]$, we say that $\vec{A}_i$ is "more stable" that $\vec{A}_j$. In a nonpotential system, on the contrary, there are different criteria to determine the relative stability of the asymptotic states. In fact, the motion of an interface between two linearly stable solutions of a dynamical system was long ago proposed as a measure of relative stability for a nonpotential system [43]. It might be said then that the most stable state will be the one that tends to overrun the other. However, this is somewhat artificial, and the nonpotential effects must in general be studied for every particular system.

Chapter 2

1d fronts between two equivalent homogeneous states

In this chapter we attempt to classify the 1d fronts between equivalent homogeneous states considering two independent properties of their profiles: the symmetries and the shape of the tails.

2.1 Front symmetries

We consider fronts in systems having translational ($\mathcal{T} : \vec{x} \rightarrow \vec{x} + \vec{x}'$) and parity ($\mathcal{P} : \vec{x} \rightarrow -\vec{x}$) invariance. We need also the system to have a discrete symmetry $\mathcal{Z}$ that allows for the existence of two equivalent solutions $\vec{A}_1$ and $\vec{A}_2$. These two solution are transformed into each other on applying $\mathcal{Z}$ ($\mathcal{Z}\vec{A}_1 = \vec{A}_2$ and $\mathcal{Z}\vec{A}_2 = \vec{A}_1$). Due to the parity invariance, for each front $\vec{A}(x)$ connecting from left to right $\vec{A}_1$ with $\vec{A}_2$, the opposite one connecting $\vec{A}_2$ with $\vec{A}_1$ in the same direction also exist, and they are transformed into each other on applying $\mathcal{Z}$. This symmetry allows us to define the center x_0 of a front $\vec{A}(x)$ as the point where $\vec{A}(x_0) = \mathcal{Z}\vec{A}(x_0)$.

Considering all these symmetry properties, following [29], we can classify the fronts connecting the two equivalent homogeneous solutions depending on the result of applying the transformation $\mathcal{S} = \mathcal{Z}\mathcal{P}_0$, where the subscript $_0$ means that the reference frame for the spatial inversion is chosen at the center of the wall x_0. Note that $\mathcal{S}\mathcal{S} = I$, with I the identity matrix. There is, then, two types of fronts:

- **Ising walls**. A front $\vec{A}(x)$ is called a Ising wall if it is invariant with respect to $\mathcal{S}$, i.e. $\mathcal{S}\vec{A}(x) = \vec{A}(x)$. We say, then, that an Ising wall is symmetric with respect to $\mathcal{S}$. Due to the symmetry, an Ising wall is always stationary.

- **Bloch walls**. In some systems, a transition from a symmetric (Ising) to two asymmetric fronts associated with a breaking of the $\mathcal{S}$ invariance occurs. Then, a couple of new asymmetric fronts $\vec{A}_+(x)$ and $\vec{A}_-(x)$ appear as solutions connecting the two homogeneous states. The symmetry operator $\mathcal{S}$ transform the two fronts into each other ($\mathcal{S}\vec{A}_+(x) = \vec{A}_-(x)$). We call these fronts Bloch walls and the $\mathcal{S}$ symmetry breaking bifurcation Ising-Bloch transition. The main feature of a Bloch wall is its asymmetry with respect to $\mathcal{S}$. The chirality is a measure of the departure of a Bloch wall from the invariance with respect to $\mathcal{S}$. A vectorial chiral order parameter $\vec{\chi}$ can be defined for a front $\vec{A}_+(x)$ as $\vec{\chi}(\vec{A}_+) = \vec{A}_+(x_0) - \vec{A}(x_0)$ where $\vec{A}(x)$ is the Ising front for the same values of the parameters. It is said that $\vec{A}_+(x)$ and $\vec{A}_-(x)$ are Bloch walls with opposite chirality since $\vec{\chi}(\vec{A}_+) = -\vec{\chi}(\vec{A}_-)$. In nonpotential systems, despite the fact of connecting equivalent states, Bloch walls usually move due to nonpotential effects. Bloch walls with opposite chirality move in opposite directions.

The definition of Ising and Bloch walls given above is a generalization of the common definition given in the literature [28], for which the order parameter vanishes at the core of a Ising wall, but not at the core of a Bloch wall.

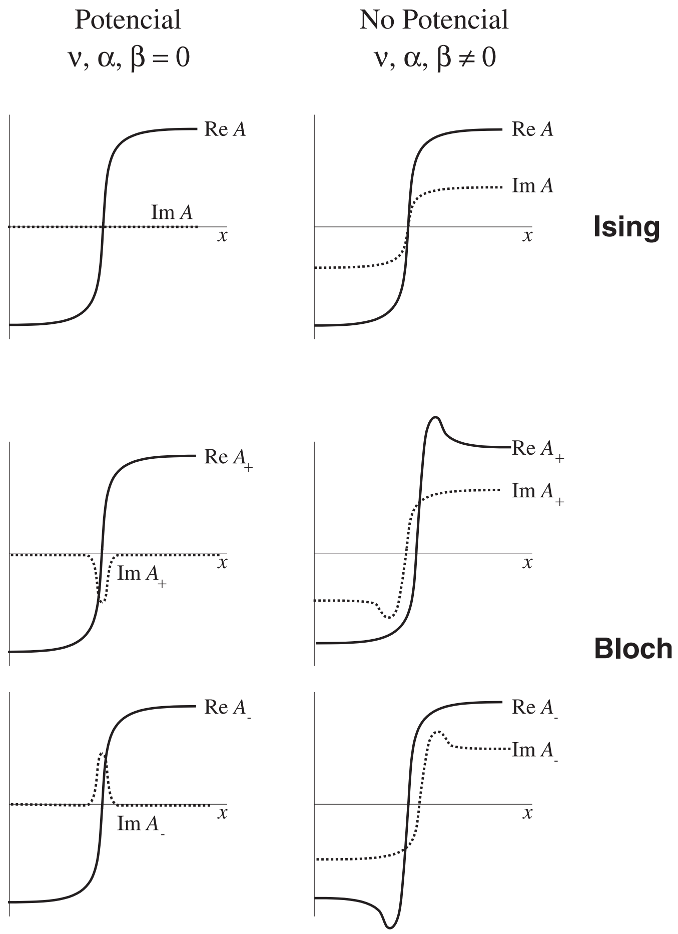

Figure 2.1: Diagram of the Ising and Bloch fronts in the potential and non-potential cases for the parametrically driven Ginzburg-Landau equation. For this equation $\mathcal{Z} : \vec{A} \to -\vec{A}$. Notice the breaking of the $\mathcal{S}$ symmetry in the Bloch solution

To illustrate the previous ideas we consider the parametrically driven complex Ginzburg-Landau equation (PCGLE) [28, 44], which is the generic amplitude equation for an oscillatory system parametrically forced at twice its natural frequency

[45]:

$$\partial_t A = (1 + i\alpha)\nabla^2 A + (\mu + i\nu)A - (1 + i\beta)|A|^2 A + pA^*\,, \tag{2.1}$$

where μ measures the distance from the oscillatory instability threshold, ν is the detuning and $p > 0$ is the forcing amplitude. This model has been used to describe a light sensitive form of the Belousov-Zhabotinsky reaction [45]. In nonlinear optics, models for vectorial Kerr cavities and optical parametric oscillators can be reduced to the PCGLE [46]. Note that $\nu, \alpha, \beta \neq 0$ prevent the possibility of a potential description of the system. For large enough values of the forcing amplitude p the system has two equivalent stable homogeneous states, the so called frequency locked solutions. In the bistability region both types of walls can be observed in the potential case as well as in the nonpotential case (see Fig. 2.1).

2.2 Front tails

It is convenient to distinguish between fronts that approach monotonically the asymptotic states and fronts whose profiles show damped oscillatory tails. The shape of the tails plays and important role in the interaction between two walls. When the front has monotonic tails the interaction between two walls is attractive, however, when the profile shows spatial oscillations, it is known that the interaction can involve both attractive and repulsive forces [18].

The existence of oscillatory tails can be determined by means of a spatial linear stability analysis of the homogeneous asymptotic solutions. A nonvanishing imaginary part of any of the resulting eigenvalues reveals the existence of oscillatory tails in the front profiles. The real part has to do with the damping rate of the oscillations. Let us see an example. For the GL equation the stationary solutions satisfy

$$\partial_{xx}\psi - V'(\psi) = 0, \tag{2.2}$$

where $V(\psi) = (1 - \psi^2)^2$. Let us call ψ_1 and ψ_2 the minima of the potential V. Writing $\psi = \psi_i + \epsilon e^{\lambda x}$, we get, upon insertion into (2.2),

$$\lambda^2 = V''(\psi_i), \quad i = 1, 2. \tag{2.3}$$

Since the ψ_i are minima of V, $V''(\psi_i) > 0$, $i = 1, 2$, so that the eigenvalues λ given by (2.3) are real. Therefore, the fronts are monotonic such as the one of Fig. 2.2 (a).

Let us consider now the Swift-Hohenberg equation (1.6). The stationary solution satisfies

$$-\partial_{xxxx}\psi - 2k_0^2\partial_{xx}\psi - V'(\psi) = 0, \tag{2.4}$$

where $V(\psi) = -(1 - k_0^4)\psi^2/2 + \psi^4/4$. The same analysis as before yields to the following four order polynomial for the eigenvalues

$$\lambda^4 + 2k_0^2\lambda^2 + 2(1 - k_0^4) = 0. \tag{2.5}$$

For $k_0^2 < \sqrt{2/3}$ there are four complex spatial eigenvalues, so that the fronts have oscillatory tails such as the one of Fig. 2.2 (b)

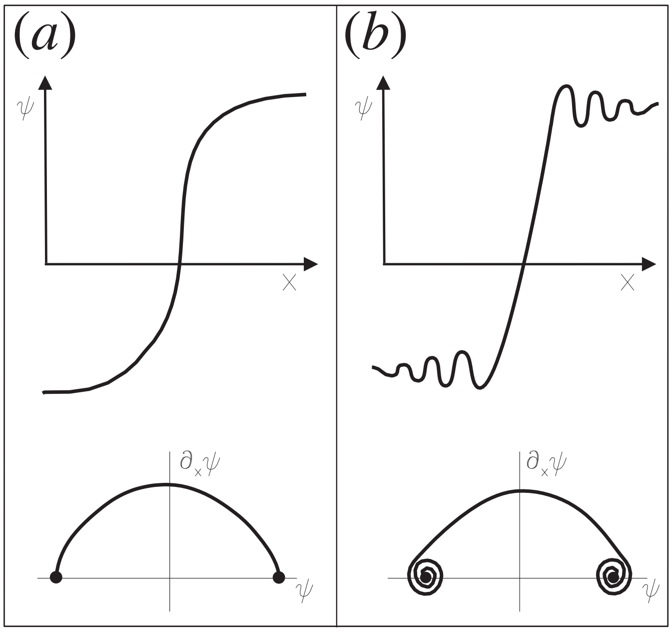

Figure 2.2: Profile of a front connecting to equivalent homogeneous states and its corresponding heteroclinic orbit in phase space for the case of a monotonic front (a) and a front showing spatial oscillations (b).

Chapter 3

Domain wall dynamics in potential systems

In this chapter we present a brief review of domain wall motion in potential systems with two spatial dimensions. We will discuss only the case of relaxational gradient potential flow, since it is the most relevant case for comparison with the nonpotential case studied in the next chapter. So, the results explained in this section apply only to systems described by nonconserved order parameters. We will restrict ourselves to interfaces connecting two equivalent stable stationary homogeneous solutions. Other cases of domain wall motion have been studied in Ref. [2, 3, 14, 26].

3.1 Curvature Driven Minimization of Surface Tension

The time evolution equation for a gradient system takes the form

$$\partial_t \Psi_i = -\frac{\delta \mathcal{F}}{\delta \Psi_i} \tag{3.1}$$

where $\mathcal{F}[\vec{\Psi}]$ is a functional of a real N components vector field $\vec{\Psi}(x, y)$. Since we are dealing with interface dynamics between two equivalent stable homogeneous solutions, we assume that, without spatial dependence, $\mathcal{F}[\vec{\Psi}]$ is a double well potential and that the two minima correspond to the two equivalent stable homogeneous solutions $\vec{\Psi}_1$ and $\vec{\Psi}_2$. We also fix the energy of the homogeneous solutions as the zero energy. Thus $\mathcal{F}[\vec{\Psi}_1] = \mathcal{F}[\vec{\Psi}_2] = 0$. In 1d, the front $\vec{\Psi}_0(x)$ connecting the two asymptotic states remains at rest. It is easy to see that the order parameter saturates exponentially far away from the wall. It follows then, that the excess or lack of energy due to the presence of the wall is located on the interface itself. We can evaluate this energy of the wall as

$$\mathcal{F}_{1d} = \mathcal{F}[\vec{\Psi}_0]. \tag{3.2}$$

In 2d, for a very large circular domain of radius R ($R \gg w$, with w the front width) the radial profile can be approximated by the 1d profile $\vec{\Psi}_0(r)$. Then the energy of the circular domain wall become [24]

$$\mathcal{F}_{2d} = 2\pi R \mathcal{F}_{1d}. \tag{3.3}$$

Thus, the potential of a large circular domain wall is equal to the 1d potential times its length. Within this approximation the sign of $\mathcal{F}_{1d}$ determines the evolution of the radius. As the system tends to minimize the potential, if $\mathcal{F}_{1d} > 0$ the domain will shrink in order to make the interface as short as possible, while if $\mathcal{F}_{1d} > 0$ (negative surface tension) the domain will growth since the presence of longer walls is energetically favored.

An expression for the velocity of large circular domain walls in a potential system can be also derived, e.g. following [1], by equating two expressions for the time evolution of the potential. First we consider that the only time dependence of the potential come through the radius

$$\frac{d\mathcal{F}}{dt} = \frac{dR}{dt}\frac{d\mathcal{F}_{2d}}{dR} = v\frac{d\mathcal{F}_{2d}}{dR}, \tag{3.4}$$

where $v = dR/dt$ is the radial velocity of the front. The second expression is, in radial co-ordinates,

$$\begin{aligned} \frac{d\mathcal{F}}{dt} &= 2\pi \int_0^\infty (\sum_{j=1}^{N} \frac{\delta \mathcal{F}}{\delta \Psi_j}\frac{\partial \Psi_j}{\partial t}) r dr \\ = -2\pi \int_0^\infty \left| \frac{\partial \vec{\Psi}}{\partial t} \right|^2 r dr &\simeq -2\pi v^2 \int_0^\infty \left| \frac{\partial \vec{\Psi}}{\partial r} \right|^2 r dr \simeq -2\pi R v^2 \int_{-\infty}^\infty \left| \frac{\partial \vec{\Psi}_0}{\partial r} \right|^2 dr \end{aligned} \tag{3.5}$$

In the last equality we have considered that $\frac{\partial \vec{\Psi}_0}{\partial r} \neq 0$ only for $r \simeq R$ and that $R \gg w$. Equating these two expressions and using (3.3) one finds for the radial velocity of large circular domains

$$\frac{dR}{dt} = -\frac{\mathcal{F}_{1d}}{\int |\frac{\partial \vec{\Psi}_0}{\partial r}|^2 dr}\frac{1}{R}. \tag{3.6}$$

The behaviour of a circular domain boundary can be generalized to that of an arbitrary shape. Assuming that the curvature of the front is sufficiently small and evaluating the two expressions (3.4) and (3.5) in the reference frame moving with the front (see section 4.2), we obtain the analogous equation to (3.6) for arbitrarily shaped domains (eikonal equation)

$$v_n = -\gamma \kappa, \tag{3.7}$$

where v_n is the normal front velocity, κ is the local curvature of the domain wall and

$$\gamma = \frac{\mathcal{F}_{1d}}{\int |\frac{\partial \vec{\Psi}_0}{\partial r}|^2 dr}. \tag{3.8}$$

This law states that interfaces move following the normal direction to each point with a velocity proportional to the mean local curvature. Since the asymptotic states are equivalent, front motion is determined purely by the local curvature. The detailed form of the potential has influence on the front profile, but has no effect on their qualitative dynamics. In contrast to what happens in one dimension an interface may move in 2d despite joining equivalent states. The existence of a surface tension entails a force per unit length, proportional to the curvature, acting at each point of the interface. This force induces the motion of the front motion with a velocity proportional to the curvature.

It is worth to discuss the two cases $\mathcal{F}_{1d} > 0$ and $\mathcal{F}_{1d} < 0$ separately. If the surface energy is positive, $\mathcal{F}_{1d} > 0$, a closed domain always tend to collapse, since it evolves by reducing the length of the surrounding interface. Reduction of the total wall length is the only way to decrease the system energy. As a consequence of this length reduction, the average domain size grows with the time and coarsening takes place. In the case of a circular domain, integration of Eq.(3.6) gives

$$R(t) = \sqrt{R(0)^2 - \gamma t}. \tag{3.9}$$

Notice that $R(t)^2 \sim t$ which give the domain growth law for this potential systems. For arbitrarily shaped domains, if there is a single characteristic scale L, the wall velocity is $v \sim dL/dt$, and the curvature $\kappa \sim 1/L$. From (3.7) we have that $L(t) \sim t^{1/2}$. The systems coarsens in a self-similar way exhibiting dynamical scaling. This means that the domain structure is, in a statistical sense, independent of time up to a global scale factor (see Fig. (3.1)). In this case, the dynamical evolution of the order parameter can be completely described by interface motion driven by curvature (surface tension).

If the surface energy is negative, $\mathcal{F}_{1d} < 0$, the system evolves increasing the length of the surrounding interface, which is the only way to decrease the system energy. A flat wall is then modulationally unstable since any small curvature induced by fluctuations will evolve in a finger increasing the wall length. As a consequence the system develops labyrinthine patterns. A circular domain will growth as $R(t)^2 \sim t$ until the boundary breaks up because of the modulational instability of the domain wall, leading to a labyrinthine pattern. Note that in this case, in contrast to what happens for positive surface tension, Eq.(3.7) is only valid at the earlier stages of gently curved fronts, since the interface proliferation lead to large curvatures and strong wall interactions. There is no asymptotic growth law for the characteristic size of the domains in this case (Fig.(3.2)).

Finally, in systems where the only spatial coupling comes through diffusion, e.g. the model A dynamics (1.3), Allen and Cahn [20] showed that the proportionality coefficient γ between the normal velocity and the curvature is constant and equal to the strength of the diffusion [3]. In other systems, e.g. those described by a SHE (1.6), the sign of $\mathcal{F}_{1d}$ may change upon variations of a control parameter leading to a transition from a coarsening regime ($\mathcal{F}_{1d} > 0$) to a regime of labyrinthine patterns ($\mathcal{F}_{1d} < 0$) [23, 24]. This situation will be studied in a more general context in the next chapter.

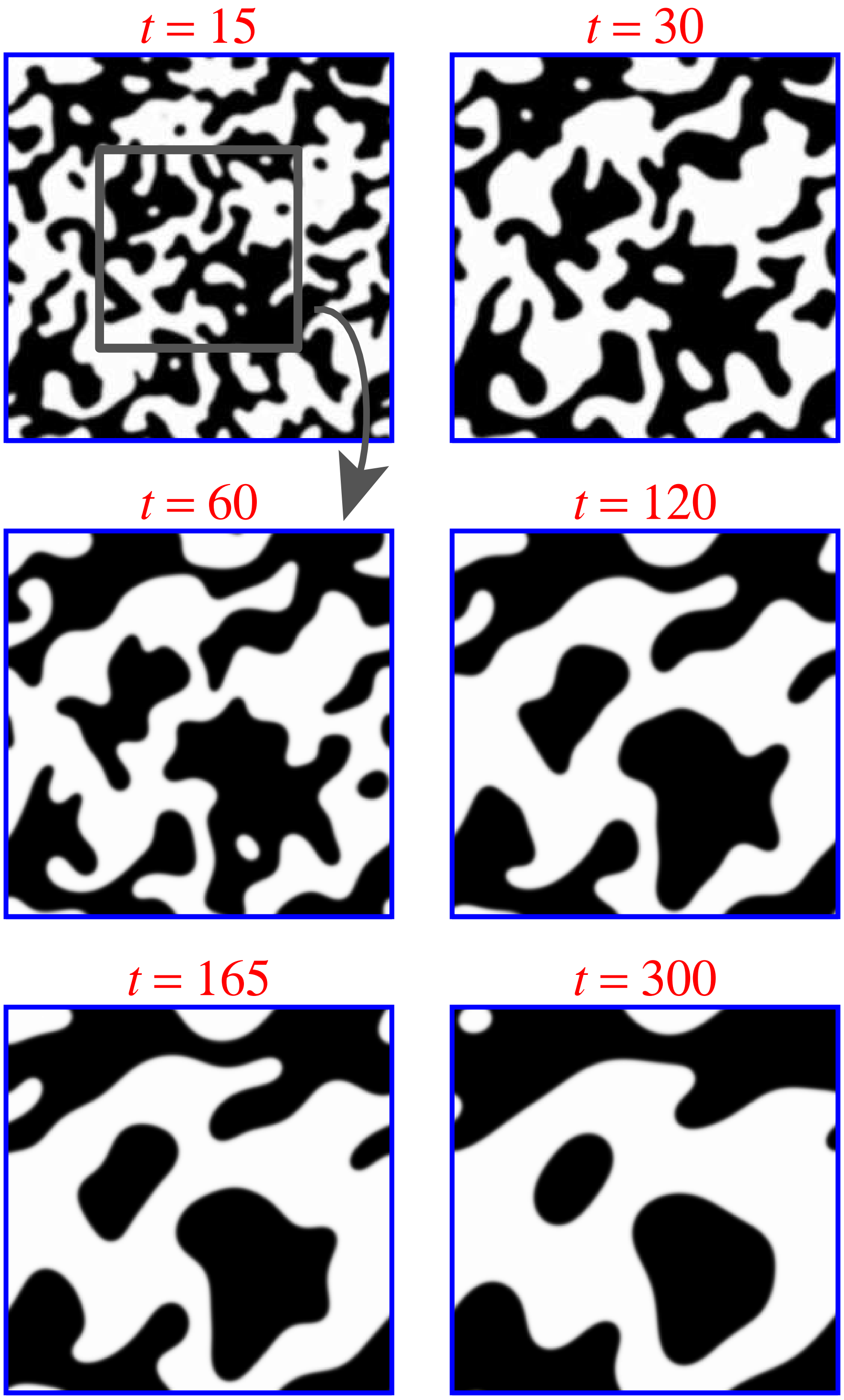

Figure 3.1: Several snapshots corresponding to a numerical simulation of a potential system described by a non-conserved order parameter (model A, equation (1.3)). In the bulk of white (black) regions the field is $+1$ (-1). The structure of domains seems to evolve self-similarly. Since the growth law for this system is $L(t) \sim t^{1/2}$, the structure of domains in a region of size A at time t will be dynamically equivalent to that of a region of size $2A$ at time $4t$ as illustrated in the figure.

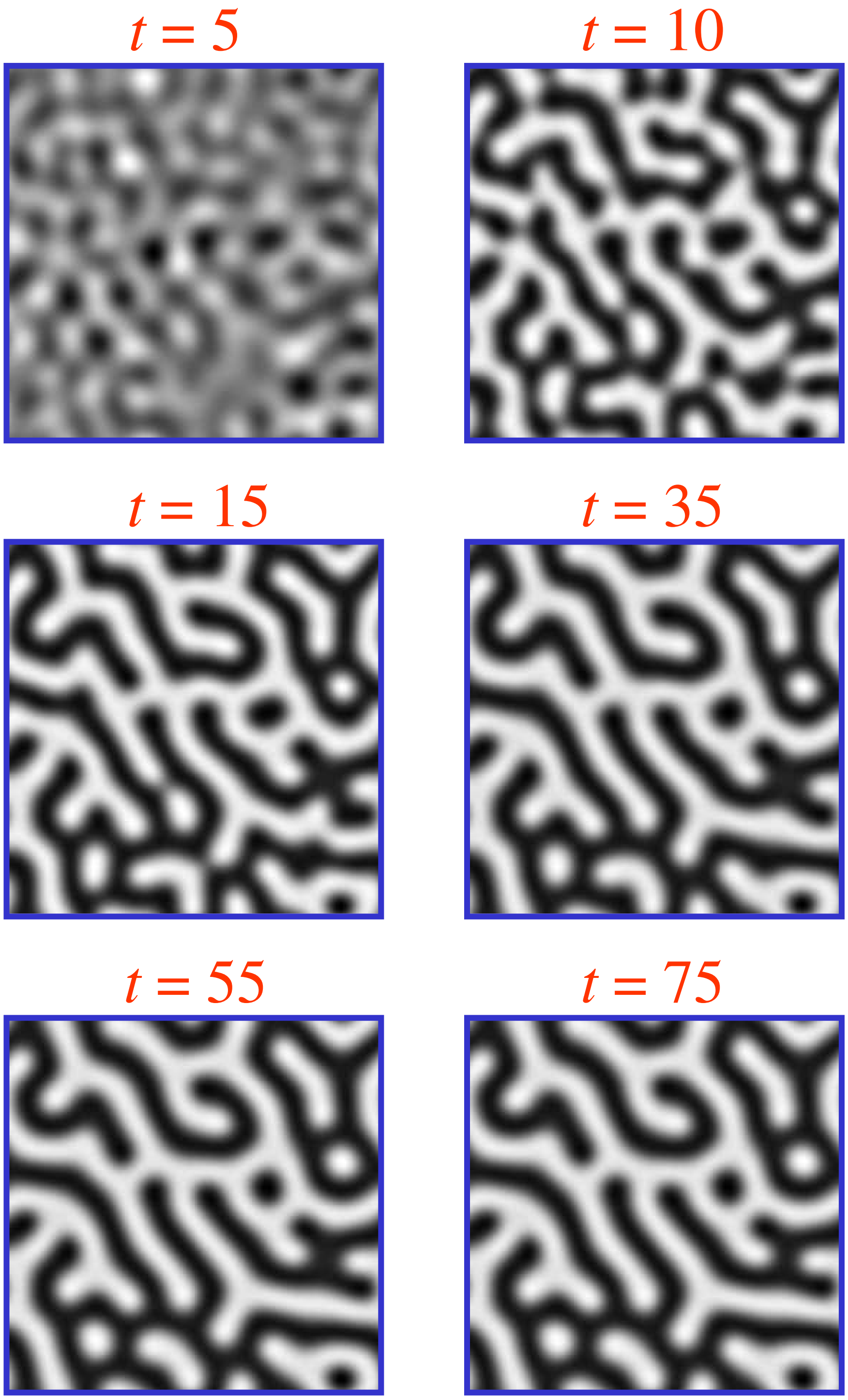

Figure 3.2: Several snapshots corresponding to a numerical simulation of a potential system described by a non-conserved order parameter (SHE, equation (1.6)). In the white (black) regions the field is around the $\sqrt{1-k_0^4}$ ($-\sqrt{1-k_0^4}$) homogeneous solution. Here $k_0 = \sqrt{0.5}$. For this value of the parameter $\mathcal{F}_{1d} < 0$ and the system develops a labyrinthine structure. In this case the structure of domains do not evolve self-similarly but reaches a nearly frozen state.

Chapter 4

Domain wall dynamics in nonpotential systems

In non-potential systems, i.e. systems whose dynamics can not be described by a equation like (1.2), being $\mathcal{F}$ a Lyapunov potential, the direct method explained in the previous chapter does not apply. Instead, we will develop in this chapter a perturbation theory for the movement of fronts connecting two equivalent homogeneous states in two spatial dimensions. This theory can be applied indistinctly to potential and non-potential systems. First we describe the systems to which our theory apply and derive a first order eikonal equation for the velocity of curved fronts. Then, we extend our analysis close to the bifurcation point where the velocity vanishes including nonlinear terms. Our general analytical results will be illustrated in the parametrically driven complex Ginzburg-Landau equation (PCGLE).

4.1 System description

We consider a system described by real N components vector field $\vec{\Psi}(\vec{x})$ whose dynamical evolution in two spatial dimensions is

$$\partial_t \vec{\Psi} = D\nabla^2 \vec{\Psi} + \vec{W}(\vec{\Psi}, p)\,, \tag{4.1}$$

where the matrix D describes the spatial coupling, $\vec{W}$ is a local nonlinear function of the fields and p a control parameter. Eq. (4.1) is invariant under translations and under the change $\mathcal{P} : \vec{x} \to -\vec{x}$ (parity). We also assume that it has a discrete symmetry $\mathcal{Z}$ that allows for the existence of two, and only two, equivalent stable homogeneous solutions, and that, in a 1d system, they are connected by a stable Ising front $\vec{\Psi}_0(x, p)$ (see chapter 2). Thus, the 1d front (and equivalently a flat front in 2d) is stationary, $D\nabla^2\vec{\Psi}_0 + \vec{W}(\vec{\Psi}_0, p) = 0$.

The PCGLE, described in chapter 2, fulfills the hypothesis required in the previous section. For $p \sim \nu \sim \alpha$ large compared to other parameters a pattern forming instability takes place for $p < p_h$, while for $p > p_h$ there are two equivalent stable homogeneous solutions (frequency locked solutions) (Fig. 4.1). The real vector

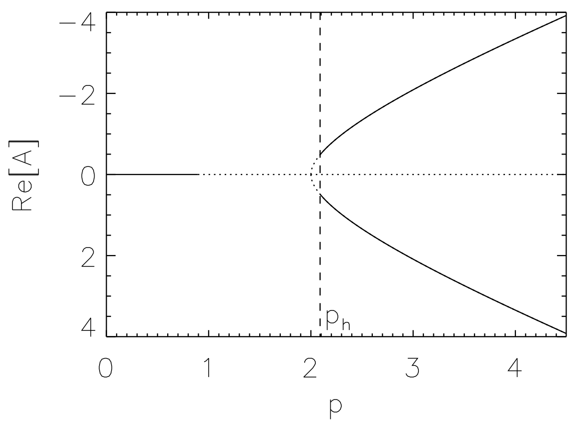

Figure 4.1: Bifurcation diagram of the homogeneous solutions of the PCGLE for $\alpha = 2$, $\beta = 0$, $\nu = 2$ and $\mu = 0$. Solid lines indicate linearly stable solutions while dotted lines indicate solutions that are unstable under finite wavelength perturbations. For the parameter values considered, $p_h = 2.09$ (dashed line).

field describing the state of the system is $\vec{\Psi}(\vec{x}) = (Re[A(\vec{x})], Im[A(\vec{x})])$, the spatial coupling is described by the matrix $D = ((1,\alpha)^T, (-\alpha, 1)^T))$, $\mathcal{Z} = -I$ and $\vec{\Psi}_0(x)$ describes a Ising front connecting the two homogeneous solutions (we consider $p > p_h$). Performing a spatial stability analysis as described in chapter 2 we obtain that the front profile has oscillatory tails as shown in Fig. 4.2.

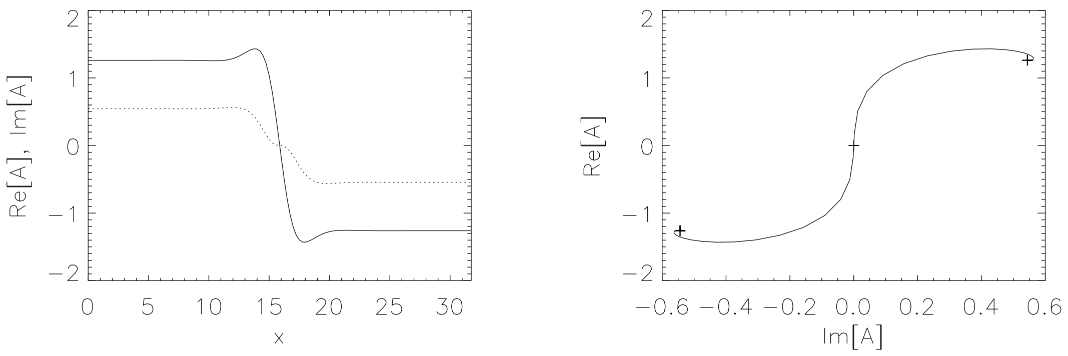

Figure 4.2: A heteroclinic solution consisting of a Ising wall for $p = 2.75$. Other parameters as in Fig. 4.1. Left: Real part (solid line) and imaginary part (dotted line) of the complex field A as a function of x in the PCGLE. The center of the wall $x_0 = 16$ is the point where the two lines cross each other, which in this case corresponds to point where the field vanishes. Note the invariance with respect to $\mathcal{S} = \mathcal{Z}\mathcal{P}_0$. Right: The domain wall plotted in the A-complex plane. The crosses indicate the two equivalent homogeneous stable solutions and the zero unstable solution.

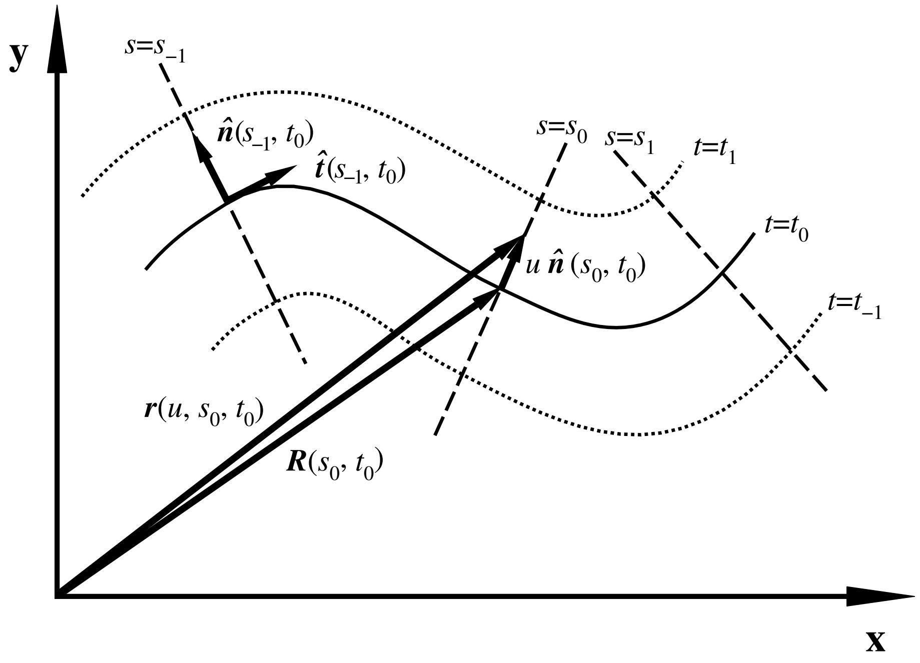

Figure 4.3: Schematic of the change of coordinates defined by Eq. (4.2).

4.2 Moving reference frame

To track the motion of the front it is useful to make a change of coordinates to an orthogonal coordinate system (u, s) that moves with the front itself [14, 47]. In the vicinity of the interface, the change of coordinates is defined by (see Fig. 4.3):

$$\mathbf{r}(u, s, t) = \mathbf{R}(s, t) + u\,\hat{\mathbf{n}}(s, t), \tag{4.2}$$

where $\mathbf{r}(u, s, t)$ is the position vector in the laboratory reference frame and $\mathbf{R}(s, t) = \big(X(s, t), Y(s, t)\big)$ is the position vector of the line front in the laboratory reference frame. The coordinate s is the arclength of the line front while u is the normal coordinate to the front. The vector $\hat{\mathbf{n}}(s, t) = Y_s\,\hat{\mathbf{x}} - X_s\,\hat{\mathbf{y}}$ is the unit normal vector to the curve, being $\hat{\mathbf{x}}$ and $\hat{\mathbf{y}}$ normal unitary vectors along the x and y axis. The subscripts indicate partial derivatives. The Jacobian matrix of the transformation is given by:

$$M(u, s, t) \equiv \frac{\partial \mathbf{r}(u, s, t)}{\partial(u, s)} = \begin{pmatrix} Y_s & X_s + uY_{ss} \\ -X_s & Y_s - uX_{ss} \end{pmatrix}. \tag{4.3}$$

The matrix of the metric defined by the change of coordinates is now easily obtained:

$$G(u, s, t) \equiv M^{\dagger}M = \begin{pmatrix} 1 & 0 \\ 0 & (1 + u\kappa)^2 \end{pmatrix}. \tag{4.4}$$

Here $\kappa(s, t)$ is the local curvature of the front line and we have used the identities:

$$\kappa(s, t) = X_s Y_{ss} \;-\; Y_s X_{ss} = \sqrt{X_{ss}^2 + Y_{ss}^2}, \tag{4.5}$$

$$X_s^2 \;+\; Y_s^2 = 1. \tag{4.6}$$

The Laplacian and the temporal derivative are transformed according to the relations:

$$\nabla^2_{u,s} = \frac{1}{G_{11}G_{22}}\left[\frac{\partial}{\partial u}\left(\sqrt{\frac{G_{22}}{G_{11}}}\frac{\partial}{\partial u}\right) + \frac{\partial}{\partial s}\left(\sqrt{\frac{G_{11}}{G_{22}}}\frac{\partial}{\partial s}\right)\right] \tag{4.7}$$

$$= \frac{\kappa}{1+u\kappa}\frac{\partial}{\partial u} + \frac{\partial^2}{\partial u^2} - \frac{u\kappa_s}{(1+u\kappa)^3}\frac{\partial}{\partial s} + \frac{1}{(1+u\kappa)^2}\frac{\partial^2}{\partial s^2}, \tag{4.8}$$

$$\frac{\partial}{\partial t} = -v_n\frac{\partial}{\partial u} - \frac{1}{1+u\kappa}\,\mathbf{r}_t\cdot\hat{\mathbf{t}}\,\frac{\partial}{\partial s} + \frac{\partial}{\partial t'}, \tag{4.9}$$

where $v_n = -\mathbf{r}_t \cdot \hat{\mathbf{n}}$ is the normal velocity, $\hat{\mathbf{t}} = X_s\,\hat{\mathbf{x}} + Y_s\,\hat{\mathbf{y}}$ is a unit vector tangent to the front line and t' is the time in the moving reference frame, which is taken equal to the time t in the laboratory reference frame. In the following we assume that the front tangent velocity term can be neglected.

4.3 Eikonal equation

In the moving frame Eq. (4.1) becomes

$$\begin{aligned} D\partial_u^2\vec{\Psi} \quad &+ \quad \left(v_n I + \frac{\kappa}{1+u\kappa}D\right)\partial_u\vec{\Psi} + \frac{u\kappa^2\partial_\theta\kappa}{(1+u\kappa)^3}D\partial_\theta\vec{\Psi} \\ &+ \quad \frac{\kappa^2}{(1+u\kappa)^2}D\partial_\theta^2\vec{\Psi} + \vec{W}(\vec{\Psi},p) = \partial_t\vec{\Psi}\,, \end{aligned} \tag{4.10}$$

where $\theta = \kappa s$ is the azimuthal angle and I the identity matrix. We analyze the dynamics of slightly curved fronts $\vec{\Psi}(u,s,t)$ as a perturbation of the flat front $\vec{\Psi}_0(u)$

$$\vec{\Psi}(u,s,t) = \vec{\Psi}_0(u) + \vec{\Psi}_1(u,s,t). \tag{4.11}$$

We assume that i) $\kappa w \ll 1$, with w the front width, ii) in the moving frame the front profile depends at most weakly on t ($|\partial_t\vec{\Psi}| \ll |\kappa D\partial_u\vec{\Psi}|$) and iii) κ is a function which depends at most weakly on s, thus $|\kappa\partial_\theta^2\vec{\Psi}| \sim |\kappa\partial_\theta\vec{\Psi}| \ll |\partial_u\vec{\Psi}|$. Linearizing around $\vec{\Psi}_0$ we have

$$M\vec{\Psi}_1 = -(vI + \kappa D)\partial_u\vec{\Psi}_0\,, \tag{4.12}$$

where $M^i_j = D^i_j\partial_u^2 + \delta_{\Psi^j}W^i|_{\vec{\Psi}_0,p}$. The last term is the functional derivative of the ith component of the nonlinear vector function $\vec{W}(\vec{\Psi},p)$ with respect to the jth component of the real vector field $\vec{\Psi}$. Due to the translational invariance of (4.1), which is broken by the presence of the front, each front has a neutrally stable mode $\vec{e}_0$ ($M\vec{e}_0 = 0$), called Goldstone mode, which has the form of the gradient of the front $\vec{e}_0 \equiv \partial_u\vec{\Psi}_0$. Thus, M is singular and there exist a condition for eq. (4.12) to have a solution, the so called solvability condition (see appendix A in Ref. [1]). The condition is obtained multiplying on the left both sides of (4.12) by the null vector of $M^\dagger$, $\vec{a}_0$:

$$\int_{-\infty}^{\infty} \vec{a}_0 \cdot (vI + \kappa D)\vec{e}_0 = 0. \tag{4.13}$$

Equation (4.13) leads to the eikonal equation

$$v_n = -\gamma(p)\kappa, \tag{4.14}$$

where

$$\gamma(p) \equiv \frac{1}{\Gamma}\int_{-\infty}^{\infty} \vec{a}_0 \cdot D\vec{e}_0 du\,, \tag{4.15}$$

and $\Gamma \equiv \int_{-\infty}^{\infty} \vec{a}_0 \cdot \vec{e}_0 du$ [1]. For a circular domain $\kappa = 1/R$ and

$$v_n = \dot{R} = -\gamma(p)/R\,. \tag{4.16}$$

From Eq. (4.12) one obtains that the front perturbation $\vec{\Psi}_1(u,t) = \kappa(t)\vec{\varphi}_1(u)$ is independent of s while the dependence on t comes only through κ. $\vec{\varphi}_1$ satisfies

$$M\vec{\varphi}_1 = -(-\gamma I + D)\vec{e}_0. \tag{4.17}$$

For systems such that the diffusion matrix is proportional to the identity, $D = dI$,

$$\gamma = \frac{1}{\Gamma}d\int_{-\infty}^{\infty} \vec{a}_0 \cdot I\vec{e}_0 du = \frac{1}{\Gamma}d\Gamma = d. \tag{4.18}$$

Thus, γ takes the constant value d independently of the profile of the front and any system parameter. In this case, the rhs of (4.17) vanishes and $\vec{\varphi}_1$ must be either zero or proportional to the Goldstone mode $\vec{e}_0$. Physically this means that the fronts translate without changing their radial profile. The front velocity is proportional to the curvature with opposite sign $v = -d\kappa$, which is the well known Allen-Cahn law [3, 20]. This law implies a coarsening regime with a $t^{1/2}$ growth law and shrinking of circular domains (Fig. 3.1).

In general, $D = dI + C$ with a non zero matrix C. C leads to a contribution to γ that depends on the profile of the front $\vec{\Psi}_0$ and therefore, on the system parameters. From Eq.(4.17) we have that $\vec{\varphi}_1$ is no longer proportional to the Goldstone mode. This means that the transverse profile of the front is now deformed. Since $\vec{\Psi}_1(u,t) = \kappa(t)\vec{\varphi}_1(u)$, the amount of deformation is proportional to the curvature and C (Fig. 4.4). The d contribution is generally positive and, for wide parameter regions, γ is also positive. Here flat walls are stable and the Allen-Cahn law still applies [10, 11] (Fig. 4.5). Circular domains shrink but in the parameter regions where the γ coefficient takes moderated values the 1d interaction due to presence of oscillatory tails in the front may prevent the droplet to disappear forming a localized structure (LS) as found in nonlinear optical cavities [10, 11, 27] (Fig. 4.6).

[1] Γ vanishes at a Ising-Bloch transition [29]. Here we only consider parameter regions far away from any Ising-Bloch transition for which Γ is never zero.

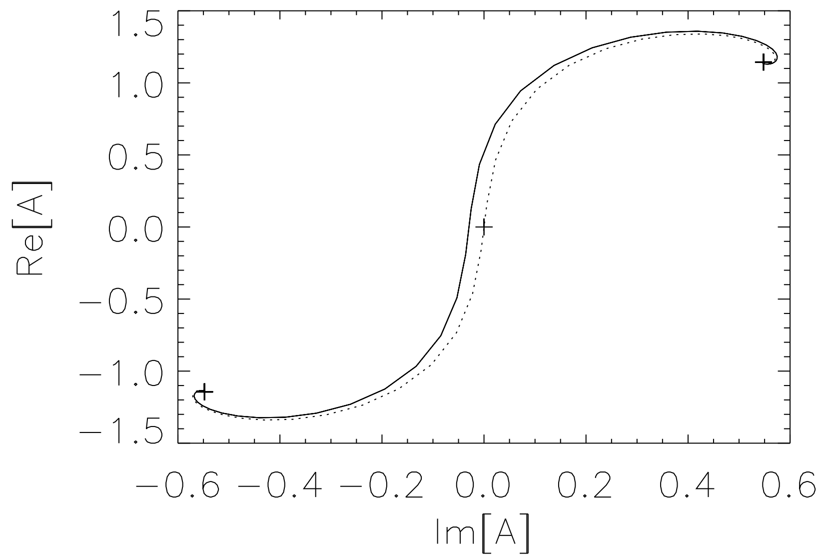

Figure 4.4: Wall profile plotted in the A-complex plane. The dotted line correspond to the 1d wall and the solid line to a slightly curved front in 2d. The symbols correspond to the zero solution and the two non-trivial homogeneous equivalent solution. The difference between the curved front and the flat wall is the effect of the deformation due to the first order correction $\vec{\Psi}_1$.

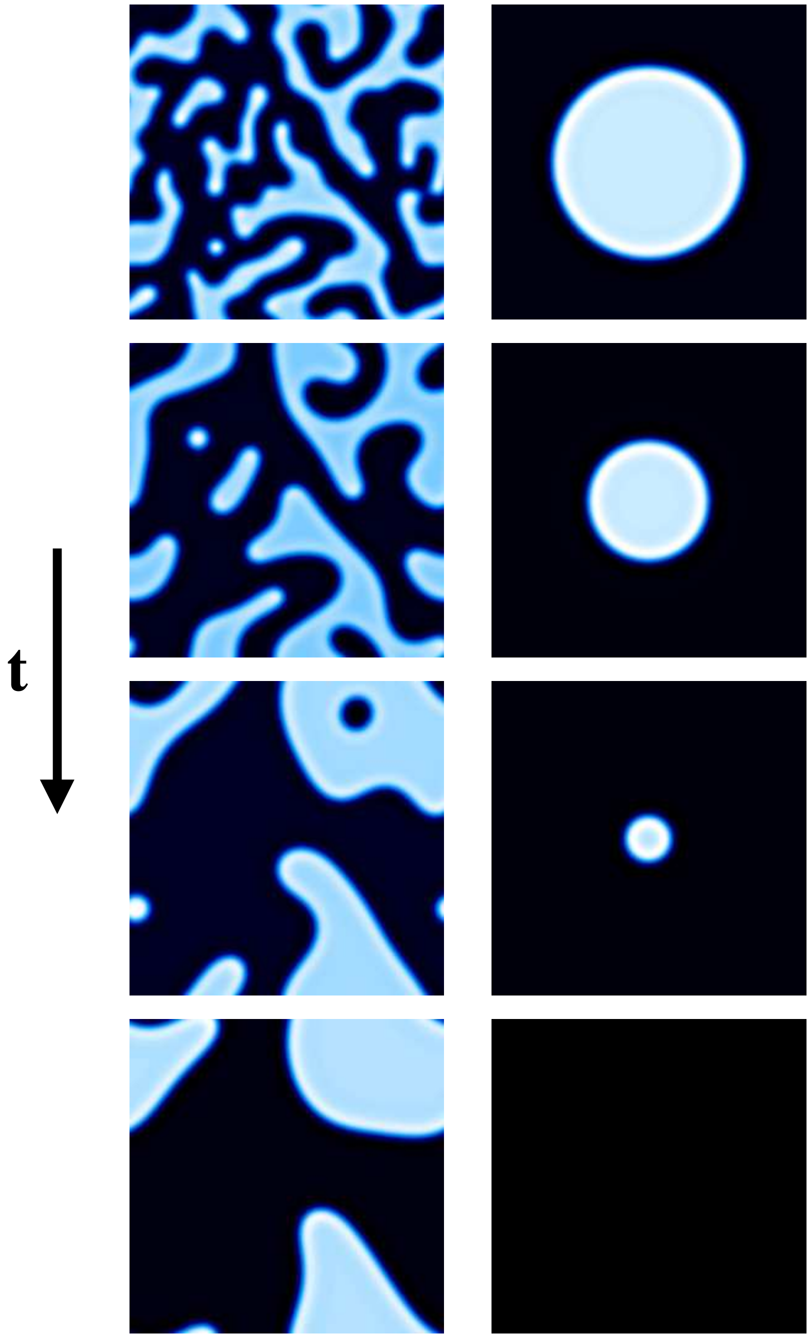

Figure 4.5: Snapshots corresponding to the time evolution of the real part of the complex field A for the parametrically driven complex Ginzburg-Landau equation in the domain coarsening regime ($\gamma > 0$). Left: evolution starting from random initial conditions. Right: evolution of an isolated circular drop.

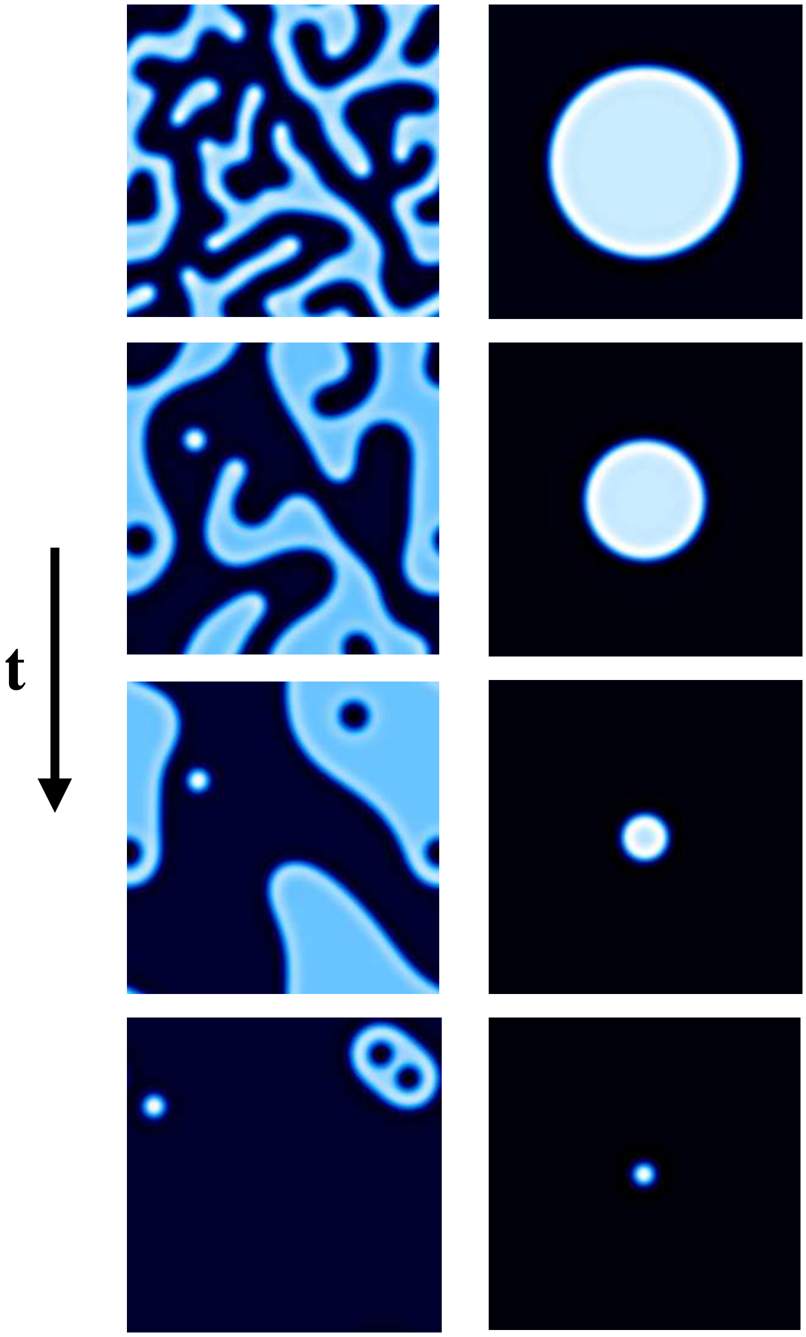

Figure 4.6: The same as Fig. 4.5 in the regime of formation of LS ($\gamma \gtrsim 0$).

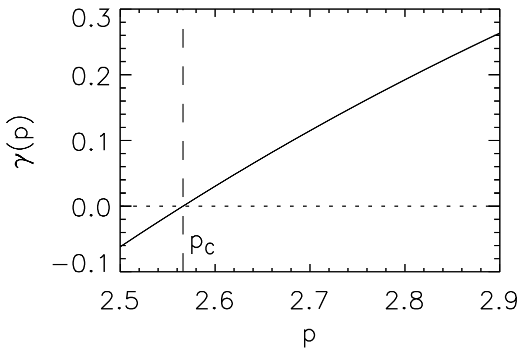

Figure 4.7: γ as function of p calculated from (4.15) for the PCGLE. Parameters taken as in Fig. 4.1. γ becomes zero at $p_c = 2.56629$ (dashed line).

The crucial point is that for some parameter values the contribution to γ due to C may be negative and larger than d. γ changes sign and a bifurcation occurs. Figure 4.7 shows the value of γ versus p for the PCGLE. The value of p for which $\gamma = 0$ identifies the bifurcation point p_c. This is particularly relevant in nonlinear optics where the spatial coupling is diffractive and therefore $d = 0$. For $\gamma < 0$ the velocity has the same sign of the curvature leading to the growth of any perturbation of the flat wall. The condition for vanishing γ, $\int_{-\infty}^{\infty} \vec{a}_0 \cdot D\vec{e}_0 du = 0$, is in fact the criterion for the modulational instability of a flat front. Modulational instabilities in fronts connecting two equivalent homogeneous states have been observed in numerical models [10, 12] (Fig. 4.8). Starting from a random initial condition, the system develops labyrinthine patterns [10, 45, 48]. Also, a circular domain grows like (4.16) until its boundary breaks up because of the modulational instability leading to the formation of a labyrinthine pattern (Fig. 4.9).

The values of γ shown in Fig. 4.7 have been calculated from its definition (4.15). The 1d front profile $\vec{\Psi}_0$ is obtained by solving the 1d stationary equation ($\partial_t A = 0$) of (2.1). This is done by discretising in space and thus obtaining a large set of coupled nonlinear equations. We use a Fast Fourier Transform (FFT) to compute the spatial derivatives in Fourier space. From a suitably chosen initial condition a multidimensional Newton method is used to find solutions of the set [49]. From the discretized profile $\vec{\Psi}_0$ we evaluate the operator M, which now takes the form of a $N \times N$ matrix with N the number of grid points. The null mode of $M^\dagger$ is easily obtained by finding the eigenmodes of the transposed of the matrix M. This process allows us to calculate γ with very high accuracy much faster than following the time evolution of a 2d circular droplet from a numerical integration of equation (2.1).

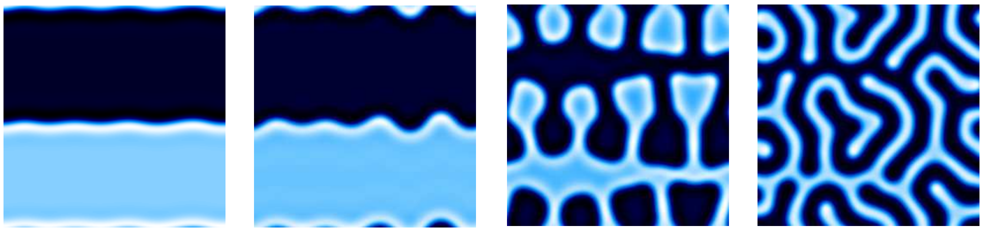

Figure 4.8: Images showing the development of a modulational instability of a flat wall for the PCGLE. The time increases from left to right.

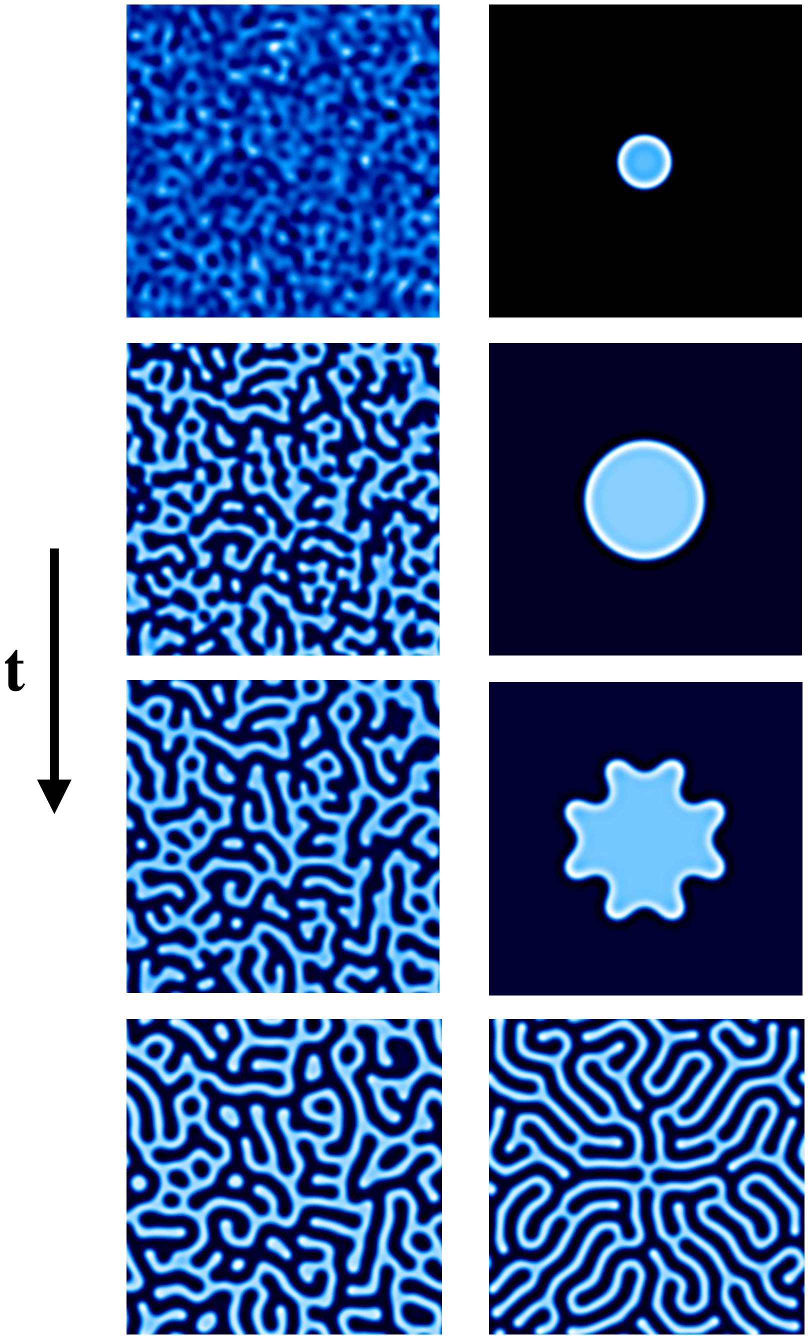

Figure 4.9: The same as Fig. 4.5 in the regime of formation of labyrinthine structures ($\gamma < 0$).

4.4 Amplitude equation for the curvature

In the previous section we have developed a perturbation theory at first order with the curvature κ. However, for values of the control parameter p close to p_c, where the proportionality coefficient γ between the velocity and the curvature vanishes (modulational instability of a domain wall), higher order contributions in κ, that have been neglected in the previous section, may become relevant. In order to study these nonlinear contributions we perform a multiple scale analysis in ϵ of Eq. (4.10). We start considering the case of a circular domain wall (for which $v_n = -\dot{\kappa}/\kappa^2$). Assuming the following scaling:

$$\begin{aligned} p &= p_c + \epsilon p_1, \\ \vec{\Psi} = \vec{\Psi}_0 &+ \epsilon^{1/2}\vec{\Psi}_1 + \epsilon\vec{\Psi}_2 + \epsilon^{3/2}\vec{\Psi}_3, \\ \kappa &= \epsilon^{1/2}\kappa_1 \quad \text{and} \\ \partial_t &= \epsilon^2 \partial_T, \end{aligned} \tag{4.19}$$

at order $\epsilon^{1/2}$ we obtain

$$M\vec{\Psi}_1 = -\kappa_1 D\vec{e}_0. \tag{4.20}$$

Now the solvability condition is $\int_{-\infty}^{\infty} \vec{a}_0 \cdot D\vec{e}_0 dr = 0$, which is precisely the criterion for the modulational instability of a domain wall, and therefore is automatically satisfied at p_c. Then a solution of (4.20) can be found:

$$\vec{\Psi}_1 = \kappa_1 \vec{\varphi}_1 \tag{4.21}$$

with $M\vec{\varphi}_1 = -D\vec{e}_0$. At order ϵ we obtain

$$M^i_j \Psi^j_2 = -p_1 \partial_p W^i|_0 - \kappa_1^2 D^i_j(\partial_u \varphi^j_1 - u e^j_0) - \frac{\kappa_1^2}{2}\delta_{\Psi^j\Psi^k} W^i|_0 \varphi^j_1 \varphi^k_1 \tag{4.22}$$

where $|_0$ means evaluated at $\vec{\Psi}_0$ and p_c, and the solvability condition is

$$\int_{-\infty}^{\infty} a_{0i} \left[p_1 \partial_p W^i|_0 + \kappa_1^2 D^i_j(\partial_u \varphi^j_1 - u e^j_0) + \frac{\kappa_1^2}{2}\delta_{\Psi^j\Psi^k} W^i|_0 \varphi^j_1 \varphi^k_1 \right] = 0. \tag{4.23}$$

$\vec{a}_0$ is antisymmetric with respect to $\mathcal{S}$, while the expression in brackets is symmetric. Therefore the integral (4.23) vanishes, so that the solvability condition at this order is always fulfilled. Then, a solution of the form

$$\vec{\Psi}_2 = p_1 \vec{\varphi}_2 + \kappa_1^2 \vec{\varphi}_3 \tag{4.24}$$

with $M\vec{\varphi}_2 = -\partial_p \vec{W}|_0$ and $M^i_j \varphi^j_3 = -D^i_j(\partial_r \varphi^j_1 - r e^j_0) - \frac{1}{2}\delta_{\Psi^j\Psi^k} W^i|_0 \varphi^j_1 \varphi^k_1$ can be found. Finally, at order $\epsilon^{3/2}$ the amplitude equation for the curvature κ_1 can be obtained from the solvability condition:

$$\frac{\partial_T \kappa_1}{\kappa_1^2} = c_1 p_1 \kappa_1 + c_3 \kappa_1^3 \tag{4.25}$$

with

$$c_1 = \frac{1}{\Gamma}\int_{-\infty}^{\infty} a_{0i}(D^i_j\partial_r\varphi^j_2 + \delta_{\Psi^j}\partial_p W^i|_0\varphi^j_1 + \delta_{\Psi^j\Psi^k}W^i|_0\varphi^j_1\varphi^k_2)dr \tag{4.26}$$

$$c_3 = \frac{1}{\Gamma}\int_{-\infty}^{\infty} a_{0i}[D^i_j(\partial_r\varphi^j_3 - r\partial_r\varphi^j_1 + r^2e^j_0) + \delta_{\Psi^j\Psi^k}W^i|_0\varphi^j_1\varphi^k_3 + \delta_{\Psi^j\Psi^k\Psi^l}W^i|_0\varphi^j_1\varphi^k_1\varphi^l_1/6]dr. \tag{4.27}$$

Equation (4.25) is written in the scaled curvature (4.19). Undoing the scaling we get

$$\frac{\partial_t\kappa}{\kappa^2} = c_1(p-p_c)\kappa + c_3\kappa^3. \tag{4.28}$$

For the radius of a circular domain ($R = 1/\kappa$) Eq. (4.28) becomes

$$\partial_t R = -c_1(p-p_c)/R - c_3/R^3. \tag{4.29}$$

$c_1 > 0$ since $\gamma = c_1(p-p_c)$, and we are considering $\gamma > 0$ for $p > p_c$. If c_3 is negative (supercritical bifurcation) our analysis predicts just above p_c the existence of stable stationary circular domains (SD) with a very large radius R_0:

$$R_0 = \frac{1}{\sqrt{p-p_c}}\sqrt{\frac{-c_3}{c_1}}. \tag{4.30}$$

In Fig. 4.10 we show the form of the SD for the PCGLE. At the SD center the field closely approaches the value of one of the homogeneous solutions so the wall of this

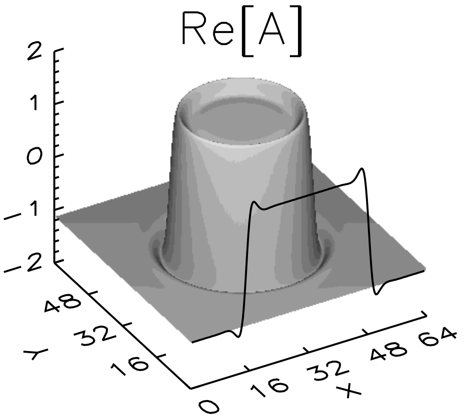

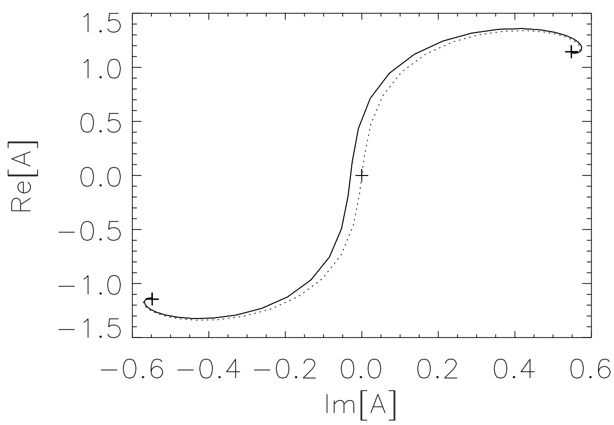

Figure 4.10: Left: spatial dependence and transverse section of a stable droplet. Right: the wall of the structure plotted in the A-complex plane (solid line). The 1d wall (dotted line) is also plotted for comparison with the wall of the stable droplet. The crosses indicate the two equivalent homogeneous solutions and the zero solution. Note that the profile of the wall of the stable droplet is slightly deformed with respect to the 1d wall due to the first order correction $\vec{\Psi}_1$.

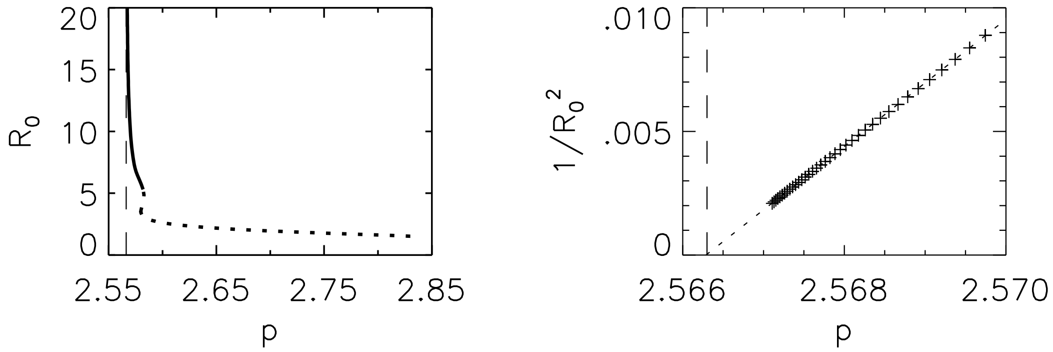

Figure 4.11: Right: Radius of SD (solid line) and LS (dotted line) as a function of the forcing p. Left: Linear dependence of $1/R_0^2$ with p close to the bifurcation point p_c (dashed line) as predicted by (4.30).

structure is very close to a heteroclinic orbit between the two homogeneous states (Fig. 4.10 (right)). The radius of the SD diverges to infinity at p_c. Figure 4.11 displays the radius of the SD and that of the LS calculated by solving numerically $(1+i\alpha)(\partial_r^2 + \frac{1}{r}\partial_r)A + (\mu + i\nu)A - (1+i\beta)|A|^2A + pA^* = 0$.

Fig. 4.11 (right) shows the linear dependence of $1/R_0^2$ with p as predicted by (4.30). In spite of the fact that there is a smooth transition from LS to SD (Fig. 4.11 (left)), they are intrinsically different. As the radius of the stable droplets is so large, the oscillatory tails interaction, responsible for the existence of LS (Fig. 4.12), does not play any role in the SD. The stabilization mechanism comes from the counterbalance between the R^{-3} contribution to the front velocity and the shrinking

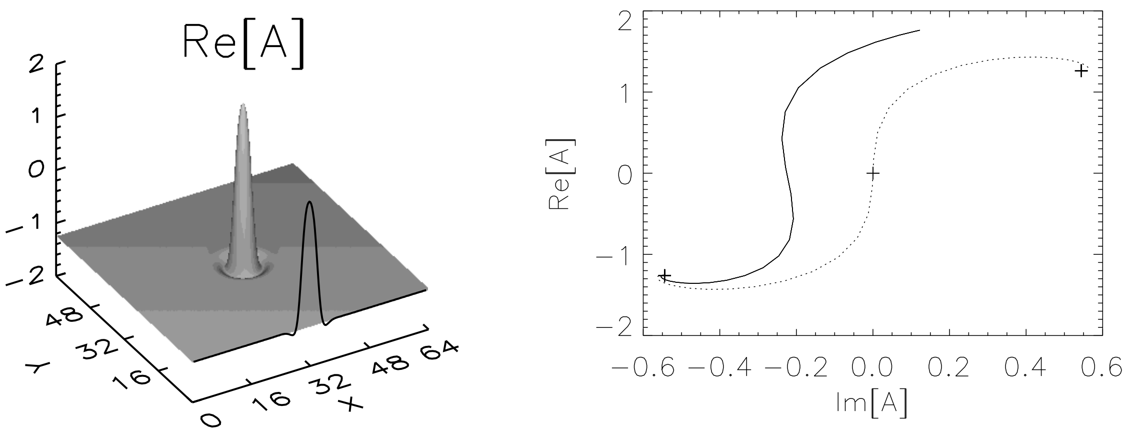

Figure 4.12: Left: spatial dependence and transverse section of a LS. Right: a cross-section of the LS plotted in the A-complex plane (solid line). The 1d wall (dotted line) is also plotted for comparison with the wall of the LS. The crosses indicate the two equivalent homogeneous solutions and the zero solution. Note that a LS can not be considered as a heteroclinic connection between the two homogeneous solutions.

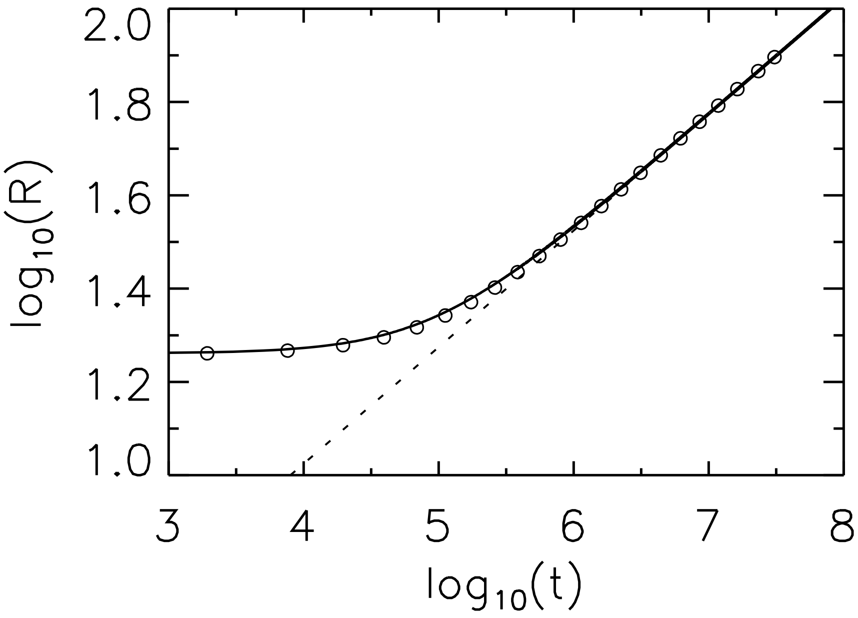

Figure 4.13: Growth of a circular domain as function of the time at $p = p_c$. Symbols correspond to the numerical integration of Eq. (2.1), the solid line is the theoretical prediction (4.29) with $c_3 = 0.3129$ calculated from (4.27) and the dotted line has a slope 1/4 showing the asymptotic behavior.

due to the R^{-1} contribution [2]. If $c_3 > 0$ (subcritical bifurcation) there would be unstable circular domains with radius R_0 just below p_c. However, we have never encountered this situation.

Another interesting feature of the nonlinear contributions of the curvature to the front velocity is the growth law of the circular domains at p_c. At p_c, Eq. (4.29) becomes

$$\partial_t R = -c_3/R^3, \tag{4.31}$$

and any circular domain of one solution embedded in the other grows as $R(t) \sim t^{1/4}$. In Fig. 4.13 we show the time evolution of the radius of a circular domain at p_c for the PCGLE. The numerical integration of eq. (2.1) (circles) fits nicely the theoretical dependence we predict (solid line). Note that, as we can calculate the value of c_3 from the solvability condition, we are able to predict not only the asymptotic power law but also the growth at earlier stages.

Close to p_c, in the regime of existence of the SD, there is no asymptotic power law of domain growth since at very long times the SD is formed stopping the growth process. During the transient, an initially small (very large) circular domain will grow (shrink) following (4.29).

[2]Crossover between different growth laws has been found in systems with conserved order parameter [50]. In that case, however, the coefficients have the same sign and there is no stationary radius for the domains.

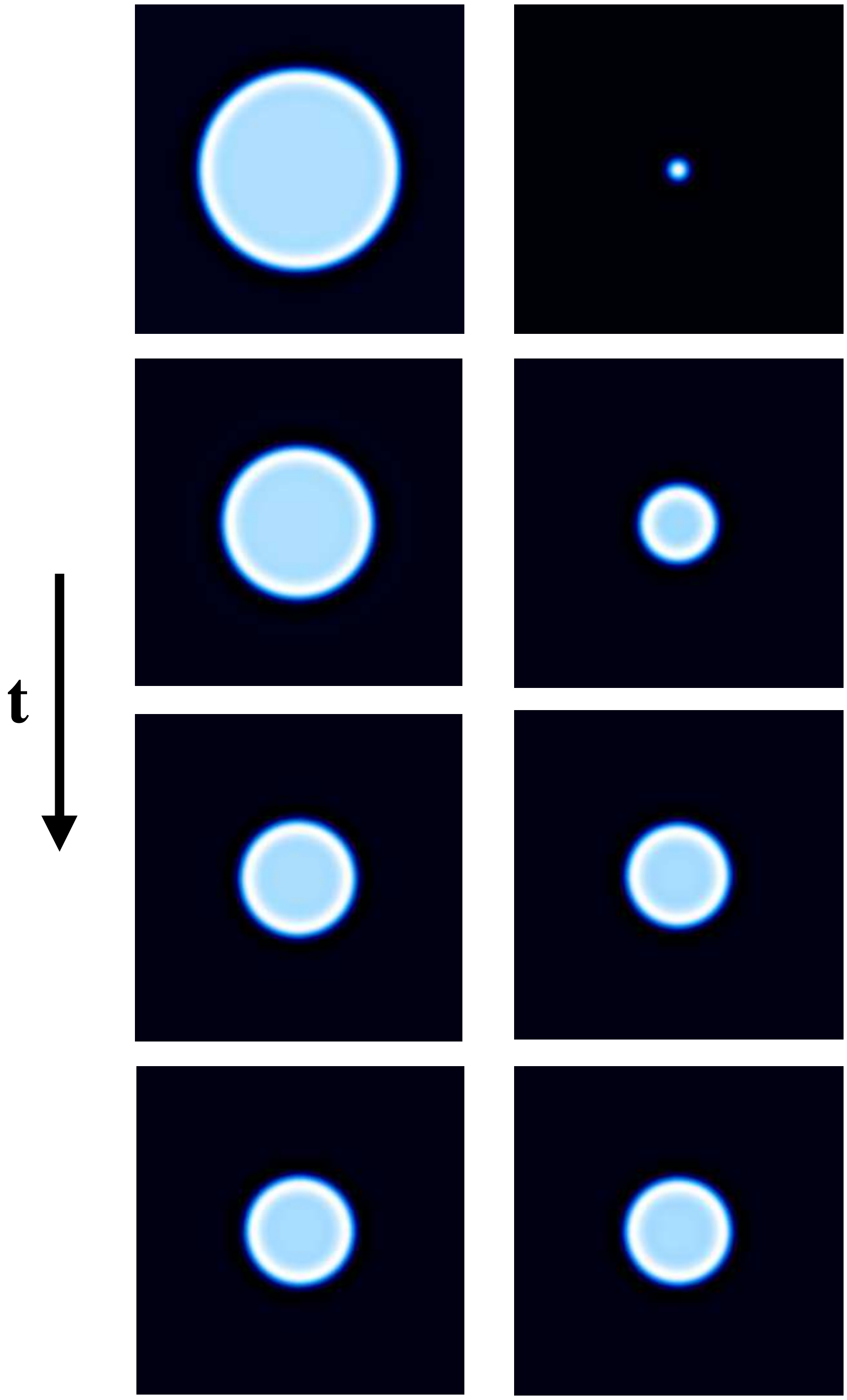

Figure 4.14: Snapshots corresponding to the time evolution of a very large and a small circular domains for the parametrically driven complex Ginzburg-Landau equation in the regime of existence of stable droplets.

So far we have considered the dynamics of domains with radial symmetry. When the system evolves from random initial conditions other dynamical mechanisms come into play. The main non-radially symmetric contribution to the velocity comes from the variation of the curvature along the front. Taking this effect into account, we can derive an amplitude equation for the normal velocity v_n. Using the fact that for circular domains $v_n = \partial_t \kappa/\kappa^2$, which is of order $\epsilon^{1/2}$, we now assume the scaling $v_n = \epsilon^{1/2} v_{n1}$. We obtain at order $\epsilon^{3/2}$ an additional term with respect to the case of radial symmetry (4.25):

$$c_2 \kappa_1^2 \partial_\theta^2 \kappa_1, \tag{4.32}$$

where $c_2 = \frac{1}{\Gamma}\int_{-\infty}^{\infty} \vec{a_0} \cdot D\vec{\varphi}_1 dr$. Thus,

$$v_{n1} = c_1 p_1 \kappa_1 + c_2 \kappa_1^2 \partial_\theta^2 \kappa_1 + c_3 \kappa_1^3. \tag{4.33}$$

Undoing the scaling, the front velocity becomes

$$v_n = -c_1(p - p_c)\kappa - c_2 \kappa^2 \partial_\theta^2 \kappa - c_3 \kappa^3. \tag{4.34}$$

Consistently with our approximations, $\partial_\theta^2 \kappa$ will change at most at order κ^0, so the non-radial contribution is at least of order κ^2. At p_c, $c_1(p-p_c)\kappa$ vanishes, and the term given by $-c_2\kappa^2\partial_\theta^2\kappa$ may be dominant compared with $c_3\kappa^3$. The front velocity is then proportional to κ^2. However, for any closed boundary

$$\int_0^{2\pi} \partial_\theta^2 \kappa = \partial_\theta \kappa |_0^{2\pi} = 0, \tag{4.35}$$

so $\partial_\theta^2 \kappa$ has to be positive in some parts of the wall and negative in others, therefore, this term does not lead to an asymptotic growth law. If $c_2 < 0$, which is the case for the PCGLE, this term tends to reduce the curvature differences, so at p_c an arbitrarily shaped domain first becomes circular until the contribution of $\partial_\theta^2 \kappa$ vanishes and then the circular domain grows as $R(t) \sim t^{1/4}$ due to the c_3 term. Fig. (4.15) shows the time evolution of an arbitrarily shaped domain at $p = p_c$ for the PCGLE. At early stages we can observe the reduction of curvature differences along the front due to the nonradially symmetric contribution, until the domain become circular. Then, the contribution from the $\partial_\theta^2 \kappa$ term vanishes and the cubic radial symmetric term makes the circular domain to grow with a $t^{1/4}$ power law (a much slower time scale).

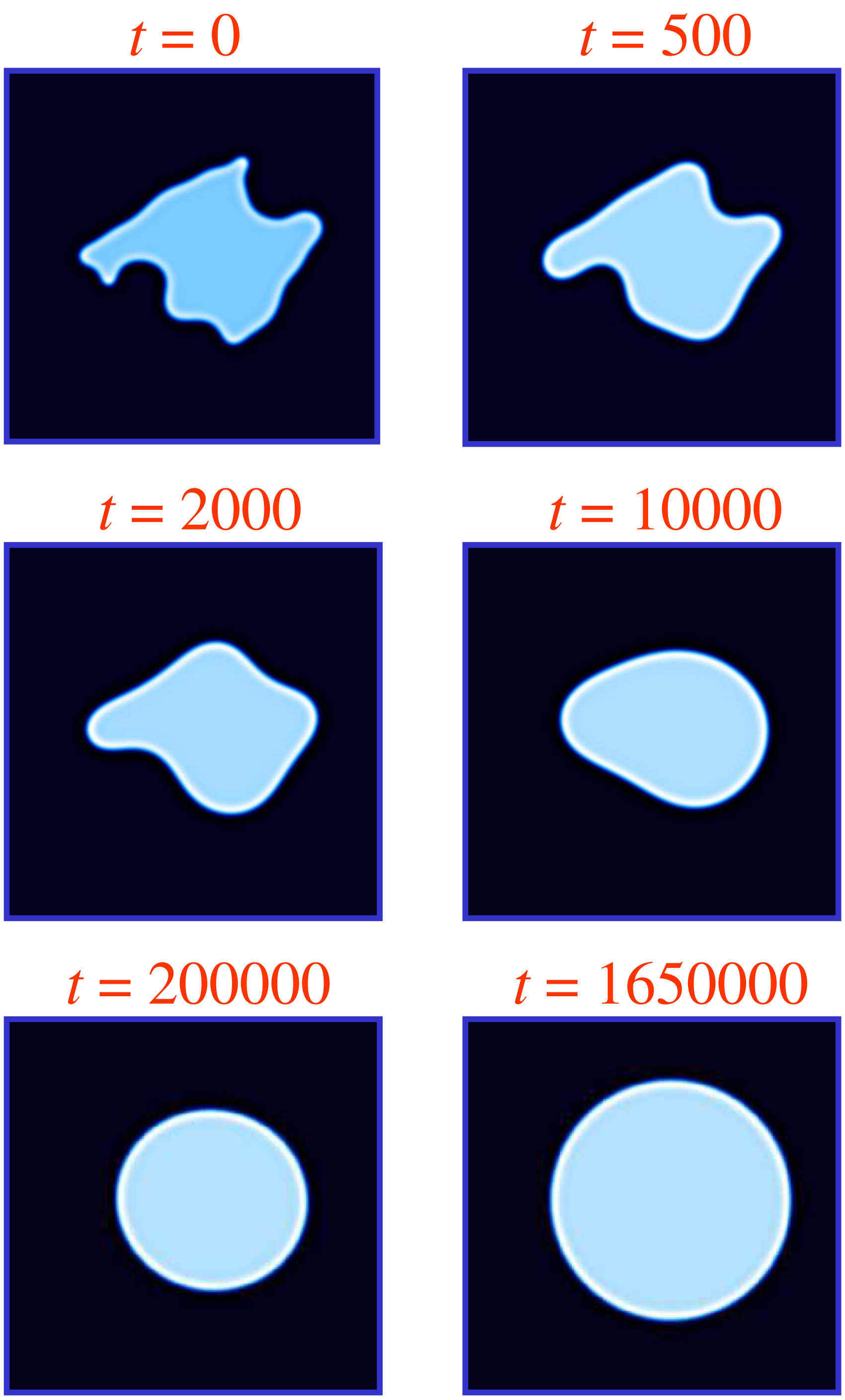

Figure 4.15: Evolution of an arbitrarily shaped domain at $p = p_c$.

Chapter 5

Conclusions and Outlook

In this work we have analyzed a generic situation of domain wall motion driven by curvature effects in which the proportionality coefficient γ between wall velocity and curvature changes sign at a bifurcation point leading to a transition from a coarsening regime (γ positive and large) to labyrinthine pattern formation ($\gamma < 0$). In the regime of coarsening the growth of domains if given by the Allen-Cahn $t^{1/2}$ power law. For γ positive but small, localized structures can be formed as consequence of the front tail interactions, therefore there is no self-similar evolution. The amplitude equation for the curvature in the vicinity of the bifurcation point predicts just above the bifurcation the existence of stable nonlinear solutions which are droplets of one phase embedded in a background of the second equivalent phase. Nonlinear dynamics of the curvature leads to growth laws different from the Allen-Cahn $t^{1/2}$ power law. The existence of a large characteristic length given by the radius of the stable droplet destroys the possibility of self-similar evolution. At the bifurcation point a $t^{1/4}$ growth law is obtained.

The determination of growth laws allows to establish from both theoretical and experimental data the mechanism that governs the dynamics of interfaces. We have explained different growth process in a framework which allow to include many nonpotential systems, for which interface dynamics is, in general, quite poorly understood. Our results come from a rigorous analysis which allow us to show in which regions of the parameter space a growth law $t^{1/2}$ or $t^{1/4}$ can be found and in which regions the system obeys a mored complicated dynamics for which the domain growth do not follow a power law.

Our results are universal in that any 2d system with a modulational instability of a flat front connecting two equivalent homogeneous states displays similar droplets and dynamics independently of the nature of the coexisting phases. Such systems can be found in fields as diverse as hydrodynamics, chemical reactions, material science and nonlinear optics. Transitions from coarsening to labyrinthine regimes has been observed experimentally in reaction diffusion [45] and optical [48] systems. Particularly relevant is the field on nonlinear optics, where the criterion for the modulational instability of a domain wall can be easily reached due to the diffractive coupling between real and imaginary parts of the complex field amplitude. In particular our general results directly apply to many models of nonlinear optical cavities such us optical parametric oscillators, self-defocusing vectorial Kerr cavities with linearly polarized input field and intracavity second harmonic generation. We are now in the process of applying our general theory to these systems [51].

The situation in which the proportionality coefficient γ between the wall velocity and curvature changes sing, commonly found in nonpotential systems, can be also found in some potential systems, generally including four order spatial derivatives, as for example the Swift-Hohenberg equation. However, the nonlinear analysis in the vicinity of the bifurcation point has never been reported for this systems.

Our analysis can be also generalized to include the case of domain walls between nonequivalent states in 2d. Basically a constant velocity v_0, coming from the movement of the domain walls in 1d, has to be added in the rhs of equation 4.14. In nonpotential systems, in general, v_0 has to be determined numerically. If v_0 is large compared with γ the main source of movement will be the 1d mechanism. Therefore the phase that overruns the other in 1d will invade the whole space in 2d. The sign of γ will determine whether the curvature acts to smooth out perturbations ($\gamma > 0$) or whether the front will be modulationally unstable ($\gamma < 0$) in the course of propagation. If ($\gamma > 0$) the curvature effect might counterbalance v_0 leading the existence of an unstable stationary radius. If v_0 is small as compared with γ, the effects of the curvature might be dominant. In this case, locally, the less favored phase may overrun the main phase due to curvature effects. Around the point where the first order contribution in κ to the front velocity counterbalances v_0, the nonlinear terms may lead, also, to the existence of SD.

A natural extension of this work would be to consider the case of Bloch walls. Two features of Bloch walls would have to be taken into account. On one hand, as in the previous paragraph, in nonpotential systems Bloch walls have a constant contribution to the velocity due to the chirality, even connecting two equivalent states in 1d. On the other hand, the symmetries of the wall profile, which are very important in the nonlinear analysis, are different from those of a Ising front. An additional difficulty would be the fact that there are defects where two Bloch walls with different chirality connect each other. This defects play an important role in the dynamics of Bloch walls and should be included in a complete theory for the movement of Bloch walls in 2d.

Bibliography

[1] M.C. Cross and P.C. Hohenberg, Rev. Mod. Phys.**65**, 851 (1993).

[2] D. Walgraef in *Spatio-Temporal Pattern Formation*, Springer-Verlag (1997).

[3] J.D. Gunton, M. San Miguel and P. Sahni in *Phase Transitions and Critical Phenomena*, edited by C. Domb and J.L. Lebowitz (Academic Press, Ney York, 1983), Vol. **8**, p. 269.

[4] J. Langer, Rev. Mod. Phys. **52**, 1 (1980).

[5] P. Meakin in *Fractals, scaling and growth far from equilibrium*, Cambridge University Press (1998); *On Growth and Form*, edited by H.E. Stanley and N. Ostrowsky (Martinus Nijhoff, Dodrechl 1986).

[6] M.C. Cross and D.I. Meiron, Phys. Rev. Lett. **75**, 2152 (1995).

[7] C. Josserand and S. Rica, Phys. Rev. Lett. **69**, 1215 (1997).

[8] R. Gallego, M. San Miguel and R. Toral, Phys. Rev. E **58**, 3125 (1998).

[9] M. Tlidi, P. Mandel and R. Lefever, Phys. Rev. Lett. **81**, 979 (1998); M. Tlidi et al., Optics Lett. **25**, 487 (2000); M. Tlidi and P. Mandel, Europhys. Lett. **44**, 449 (1998).

[10] R. Gallego, M. San Miguel and R. Toral, Phys. Rev. E **61**, 2241 (2000).

[11] G.-L. Oppo, A.J. Scroggie and W. Firth, J. Opt. B **1**, 133 (1999); Phys. Rev. E to be published (2001); G.-L. Oppo et al., J. Mod. Opt. **47**, 2005 (2000).

[12] U. Peschel et al., Phys. Rev. E **58**, R2745 (1998).

[13] M. Le Berre, E. Ressayre, and A. Tallet, J. Opt. B **2**, 347 (2000)

[14] R. Gallego, PhD Thesis (2000).

[15] S.-K. Chan, J. Chem. Phys. **67**, 5755 (1977).

[16] Y. Pomeau, Physica (Amsterdam) **23D**, 3 (1986).

[17] K. Kawasaki and T. Ohta, Physica A **116**, 573 (1982).

[18] P. Coullet, C. Elphick, and D. Repaux, Phys. Rev. Lett. **58**, 431 (1987)

[19] R. Smoluchowski, Phys. Rev. **83**, 69 (1951); D. Turnbull, Trans. Mettal. Soc. AIME **191**, 661 (1951); I.M. Lifshitz Sov. Phys. JETP **15**, 939 (1962).

[20] S.M. Allen and J.W. Cahn, Acta Metall. **27**, 1085 (1979).

[21] I. Lifshitz and V.V. Slyozov, J. Phys. Chem. Solids **19**, 35 (1961).

[22] R.E. Goldstein, D.J. Muraki and D.M. Petrich, Phys. Rev. E **53**, 3933 (1996).

[23] K. Ouchi and H. Fujisaka, Phys. Rev. E **54**, R3895 (1996)

[24] K. Staliunas and V.J. Sánchez-Morcillo, Phys. Lett. A **241**, 28 (1998); V.J. Sánchez-Morcillo and K. Staliunas Phys. Rev. E **60**, 6153 (1999).

[25] K.R. Elder, J. Viñals, and M. Grant, Phys. Rev. Lett. **68**,3024 (1992); D. Boyer and J. Viñals, preprint (2001).

[26] E. Meron, Phys. Rep. **218**, 1 (1992).

[27] M. Le Berre et al, J. Opt. B **1**, 153 (1999); P.L. Ramazza et al, ibid. **2**, 399 (2000).

[28] P. Coullet, et al., Phys. Rev. Lett. **65**, 1352-1355 (1990).

[29] D. Michaelis et al, Phys. Rev. E **63**, 066602 (2001).

[30] J. Guckenheimer and P. Holmes, *Nonlinear Oscillations, Dynamical Systems and Bifurcations of Vector Fields*, Springer–Verlag (1983).

[31] R. Montagne, E. Hernández-García, and M. San Miguel, Physica D **96**, 47 (1996).

[32] M. San Miguel and R. Toral, in *Stochastic Effects in Physical Systems, Instabilities and Nonequilibrium Structures* VI, Ed. E. Tirapegui and W. Zeller, Kluwer Academic, 1999.

[33] A. Turing, Philos. Trans. R. Soc. London B **237**, 37 (1952).

[34] J. Swift and P.C. Hohenberg, Phys. Rev. A **15**, 319 (1977).

[35] P. Mandel, M. Georgiou and T. Erneux, Phys. Rev. A **47**, 4277 (1993); V.J. Sánchez-Morcillo and G.J. de Valcárcel, Quantum Semiclass. Opt. **8**, 919 (1996).

[36] G.J. de Valcárcel et al, Phys. Rev. A **54**, 1609 (1996).

[37] R. Graham and T. Tél, Phys. Rev. A **42**, 4661 (1990).

[38] R. Graham in *Instabilities and Nonequilibrium Structures*, E. Tirapegui and D. Villarroel, eds. Reidel, Dordrecht (1993).

[39] R. Graham in *Instabilities and Nonequilibrium Structures III*, E. Tirapegui and W. Zeller, eds. Reidel, Dordrecht (1991)

[40] R. Graham in *25 years of Nonequilibrium Statistical Mechanics*, J. Brey, J. Marro, J.M. Rubi and M. San Miguel, eds. Springer Verlag (1995).

[41] O. Descalzi and R. Graham, Phys. Lett. A **170**, 84 (1992).

[42] O. Descalzi and R. Graham, Z. Phys. B **93**, 509 (1994).

[43] L. Kramer, Z. Phys. B **41**, 357 (1981); Ibíd. **45**, 167 (1981).

[44] P. Coullet and K. Emilsson, Physica D, **61**, 119 (1992).

[45] V. Petrov, Q. Ouyang and H.L. Swinney, Nature **388**, 655 (1997).

[46] V.J. Sánchez-Morcillo et al., Optics Lett. **25**, 957 (2000); K. Staliunas, J. Mod. Opt. **42**, 1261 (1995).

[47] H. Tutu, Phys. Rev. E **56**, 5036 (1997).

[48] V.B. Taranenko, K. Staliunas, and C.O. Weiss, Phys. Rev. Lett. **81**, 2236 (1998).

[49] W.J. Firth and G.K. Harkness, Asian J. Phys (1998).

[50] A.M. Lacasta, et al., Phys. Rev. B, **45** 5276 (1991).

[51] D. Gomila, P. Colet, G.-L. Oppo and M. San Miguel, preprint (2001).